AD-A096 095 PERKIN-ELMER CORP NORWALK CONN F/G 9/5
ELECTROMAGNETIC ACTUATORS.(U)
JAN 81 S ADELMAN F29601-79-C-0054
UNCLASSIFIED PE-14490 AFWL-TR-79-190 NL

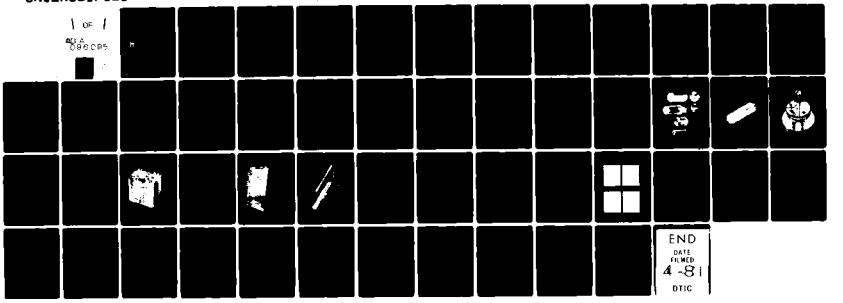

AFWL-TR-79-190

AFWL-TR-
79-190

ELECTROMAGNETIC ACTUATORS

S. Adelman

Perkin-Elmer Corporation
Main Avenue
Norwalk, CT 06856

January 1981

Final Report

AIR FORCE WEAPONS LABORATORY
Air Force Systems Command
Kirtland Air Force Base, NM 87117

This final report was prepared by the Air Force Weapons Laboratory, Kirtland Air Force Base, New Mexico, under Job Order ILIR7913. Dr John R. Kenemuth (ARAA) was the Laboratory Project Officer-in-Charge.

When US Government drawings, specifications, or other data are used for any purpose other than a definitely related Government procurement operation, the Government thereby incurs no responsibility nor any obligation whatsoever, and the fact that the Government may have formulated, furnished, or in any way supplied the said drawings, specifications, or other data, is not to be regarded by implication or otherwise, as in any manner licensing the holder or any other person or corporation, or conveying any rights or permission to manufacture, use, or sell any patented invention that may in any way be related thereto.

This report has been reviewed by the Public Affairs Office and is releasable to the National Technical Information Service (NTIS). At NTIS, it will be available to the general public, including foreign nations.

This technical report has been reviewed and is approved for publication.

John R Kenemuth

JOHN R. KENEMUTH, PhD
Project Officer

James D. Dillow

JAMES D. DILLOW
Lt Colonel, USAF
Chief, Advanced Beam Control Branch

FOR THE DIRECTOR

David W Seegmiller

DAVID W. SEEGMILLER
Colonel, USAF
Chief, Advanced Laser Tech Division

DO NOT RETURN THIS COPY. RETAIN OR DESTROY.

UNCLASSIFIED

SECURITY CLASSIFICATION OF THIS PAGE (When Data Entered)

REPORT DOCUMENTATION PAGE	READ INSTRUCTIONS BEFORE COMPLETING FORM
1. REPORT NUMBER: AFWL-TR-79-190	2. GOVT ACCESSION NO.: AD-A096095
3. RECIPIENT'S CATALOG NUMBER:	
4. TITLE (and Subtitle): ELECTROMAGNETIC ACTUATORS	5. TYPE OF REPORT & PERIOD COVERED: Final Report
	6. PERFORMING ORG. REPORT NUMBER: PE-14490
7. AUTHOR(s): S. Adelman	8. CONTRACT OR GRANT NUMBER(s): F29601-79-C-0054
9. PERFORMING ORGANIZATION NAME AND ADDRESS: Perkin-Elmer Corporation, Main Avenue, Norwalk CT 06856	10. PROGRAM ELEMENT, PROJECT, TASK AREA & WORK UNIT NUMBERS: 61101F & 63605F/ILIR7913
11. CONTROLLING OFFICE NAME AND ADDRESS: Air Force Weapons Laboratory (ARAA), Kirtland Air Force Base, NM 87117	12. REPORT DATE: January 1981
	13. NUMBER OF PAGES: 48
14. MONITORING AGENCY NAME & ADDRESS (if different from Controlling Office)	15. SECURITY CLASS. (of this report): UNCLASSIFIED
	15a. DECLASSIFICATION DOWNGRADING SCHEDULE

16. DISTRIBUTION STATEMENT (of this Report)

Approved for public release; distribution unlimited.

17. DISTRIBUTION STATEMENT (of the abstract entered in Block 20, if different from Report)

18. SUPPLEMENTARY NOTES

19. KEY WORDS (Continue on reverse side if necessary and identify by block number)

Actuator
Deformable Mirror

20. ABSTRACT (Continue on reverse side if necessary and identify by block number)

An electromagnetic actuator was configured, designed and constructed, as a direct replacement for the PZT devices now being used in deformable mirrors. The subject actuator has a stroke of +1.5 λ at 10.6 μm, and is complete with a matching amplifier so that it can readily interface into existing equipment. A magnetic circuit of Hyperco-50 iron, two BeCu flexures, and a tungsten push rod are used to construct an actuator with the required characteristics. Two amplifiers, one a linear device and the other a switching amplifier, are also

(Over)

DD FORM 1 JAN 73 1473

UNCLASSIFIED

SECURITY CLASSIFICATION OF THIS PAGE (When Data Entered)

20. ABSTRACT (Continued)

described. During the program, the device was assembled and tested, and when several structural shortcomings were observed, the push rod threads were reworked to provide additional integrity.

The actuator test results are described including test results on both amplifiers. These test results show that the device performance was as per initial predictions until the device was installed in the test cell and the full output force was placed on the push rod. Performance then deteriorated as the threads degraded.

Test results after the thread rework indicated that the device is capable of stated performance.

TABLE OF CONTENTS

LIST OF FIGURES

Conversion factors for U.S. customary
to metric (SI) units of measurement.

(Symbols of SI units given in parentheses)

To convert from	to	Multiply by
angstrom	meters (m)	1.000 000 X E -10
atmosphere (normal)	kilo pascal (kPa)	1.013 25 X E +2
bar	kilo pascal (kPa)	1.000 000 X E +2
barn	meter^2 (m^2)	1.000 000 X E -28
British thermal unit (thermochemical)	joule (J)	1.054 350 X E +3
calorie (thermochemical)	joule (J)	4.184 000
cal (thermochemical)/cm^2	mega joule/m^2 (MJ/m^2)	4.184 000 X E -2
curie	giga becquerel (GBq)*	3.700 000 X E +1
degree (angle)	radian (rad)	1.745 329 X E -2
degree Fahrenheit	degree kelvin (K)	$t_K = (t_{°F} + 459.67)/1.8$
electron volt	joule (J)	1.602 19 X E -19
erg	joule (J)	1.000 000 X E -7
erg/second	watt (W)	1.000 000 X E -7
foot	meter (m)	3.048 000 X E -1
foot-pound-force	joule (J)	1.355 818
gallon (U.S. liquid)	meter^3 (m^3)	3.785 412 X E -3
inch	meter (m)	2.540 000 X E -2
jerk	joule (J)	1.000 000 X E +9
joule/kilogram (J/kg)(radiation dose absorbed)	Gray (Gy)**	1.000 000
kilotons	terajoules	4.183
kip (1000 lbf)	newton (N)	4.448 222 X E +3
kip/inch^2 (ksi)	kilo pascal (kPa)	6.894 757 X E +3
ktap	newton-second/m^2 (N-s/m^2)	1.000 000 X E +2
micron	meter (m)	1.000 000 X E -6
mil	meter (m)	2.540 000 X E -5
mile (international)	meter (m)	1.609 344 X E +3
ounce	kilogram (kg)	2.834 952 X E -2
pound-force (lbf avoirdupois)	newton (N)	4.448 222
pound-force inch	newton-meter (N-m)	1.129 848 X E -1
pound-force/inch	newton/meter (N/m)	1.751 268 X E +2
pound-force/foot^2	kilo pascal (kPa)	4.788 026 X E -2
pound-force/inch^2 (psi)	kilo pascal (kPa)	6.894 757
pound-mass (lbm avoirdupois)	kilogram (kg)	4.535 924 X E -1
pound-mass-foot^2 (moment of inertia)	kilogram-meter^2 (kg-m^2)	4.214 011 X E -2
pound-mass/foot^3	kilogram/meter^3 (kg/m^3)	1.601 846 X E +1
rad (radiation dose absorbed)	Gray (Gy)**	1.000 000 X E -2
roentgen	coulomb/kilogram (C/kg)	2.579 760 X E -4
shake	second (s)	1.000 000 X E -8
slug	kilogram (kg)	1.459 390 X E +1
torr (mm Hg, 0° C)	kilo pascal (kPa)	1.333 22 X E -1

*The becquerel (Bq) is the SI unit of radioactivity; 1 Bq = 1 event/s.
**The Gray (Gy) is the SI unit of absorbed radiation.

A more complete listing of conversions may be found in "Standard for Metric Practice,", American Society for Testing and Materials, ASTME-380-76C.

I. OPTIMIZATION STUDY

1.1 STATEMENT OF PROBLEM

In a typical deformable mirror application, the mirror surface figure is controlled by a servo loop, and must be distorted or adjusted in response to an external command. The actuator must generally move the surface of the mirror on the order of two to three wavelengths. Force requirements are on the order of 10 to 100 pounds. Resolution requirements vary with the specific application, with a resolution of several millionths of an inch considered to be quite good.

The electromagnetic actuator should be responsive to these requirements, and provide low hysteresis, low power consumption, and the potential for a longer stroke, if required.

1.2 CHARACTERISTICS OF ELECTROMAGNETIC ACTUATORS

It has been suggested that actuators can be constructed using magnetic tractive force as the generating mechanism. These tractive force actuators can be configured to be capable of high forces over reasonable strokes. The technology which is utilized in these devices has been refined over a number of years, and is well understood. The technical issues which are involved are all related to several new magnetic materials and to the fabrication and handling of these materials, as well as to the fabrication of very precise beryllium-copper flexures.

Basically, the device which is being configured under this program consists of a cup magnet assembly and an armature suspended from a spring mechanism. The characteristics of the device will be determined by its construction and the properties of the materials which are to be utilized.

A schematic of the device is shown in Figure 1. The drive coil induces magnetic flux in the center pole piece, and the flux flows through the armature and returns through the rim. When magnetic flux is induced across a gap, the two pieces of metal are attracted. This tractive force is given by:

$$F = \frac{AB^2}{11.18} \times 10^{-6} \qquad (1)$$

where F = force in pounds

A = surface area in cm^2

B = flux density in lines/cm^2

and, the flux density is a function of gap length, and is given by:

$$B = \frac{1.26\ NI}{R} \qquad (2)$$

where:

N = No. of turns on coil

I = drive current in amperes

R = gap length in cm

The device is round, with a thin outer rim and a round center pole piece. This form factor has been chosen to ensure that the electromagnetic traction motor will be compatible with existing hardware.

1.3 DESIGN CONSIDERATIONS

The performance of a traction motor can be calculated using the two basic magnetic circuit design Equations 1 and 2. Conversely, a device can be configured using the same basic equations. In an actual design, there are several additional factors which must be considered in order to account for non-ideal behavior, and for material anomalies. The basic equations assume that all flux in the magnetic circuit passes straight through the air gap, through the armature, and through the rim and center pole. This is approximately true for very small air gaps, where the reluctance of the gap is low, and fringing of the field in the gap is small. As the initial gap increases, because of longer stroke requirements, the reluctance of the gap increases correspondingly, and part of the flux tends to leak between the center post and the outside rim. In addition, fringing begins to occur, and the flux lines do not cross the gap perpendicular to the surface of the gap. Because of these phenomena, it is necessary to apply a correction factor which is a function of the device size and geometry. The determination of some appropriate correction factors has been made by employing a vector magnetic field simulation to calculate exact device performance, and comparing this performance to calculated ideal performance and to experimental results. This simulation was done under a previous program.

In order to complete the design of the traction motor actuator, the correction factor is estimated from the device geometry, and entered into the basic equations as a force multiplier. The maximum flux density, which is a function of the material used in the magnetic circuit, and the corrected peak force are combined to determine the necessary tractive area. The total force is the sum of the force exerted by the center pole and by the outer rim. For a given total area, maximum force is realized when the center post area is exactly equal to the rim

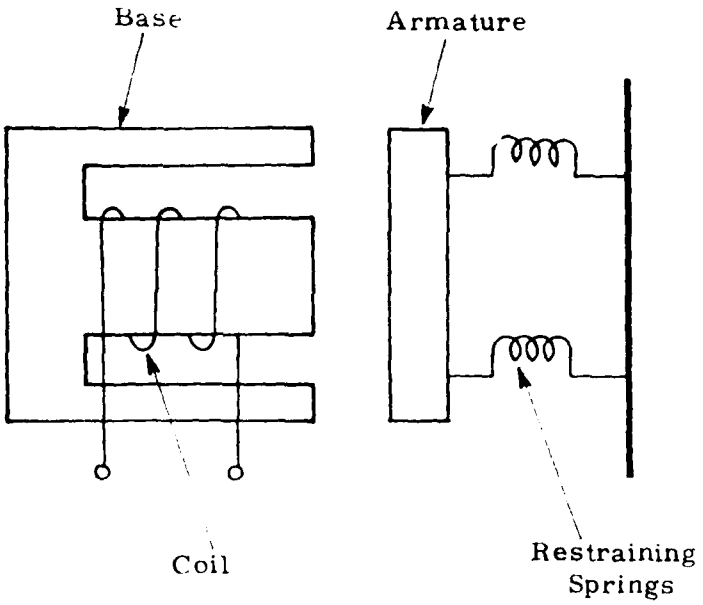

Figure 1. Schematic of Electromagnetic Actuator

area. Next, the coil and drive requirements are determined by using Equation 2. As a rule, the more wire that is used, the lower the overall power dissipation will be. However, as the amount of wire is increased, the size of the actuator increases. The final current requirements are determined from the maximum flux density, number of turns, and the initial gap.

1.3-1 MAGNETIC CIRCUIT CHARACTERISTICS

Since the force between the armature and the base is proportional to the square of the flux density, it is necessary to maximize the flux density which can be generated across the gap. There are alloys which are formulated to support high flux densities and maintain high permeabilities. The properties of these alloys are generally established not only by their composition and manufacture, but by the application of a very precise heat treating process which is applied after the material is machined to shape. As a general rule, the better the

magnetic properties of an alloy, the harder it is to machine and tread. Additionally, the alloys generally have poor structural properties, and the configuration usually must contain a support structure. A number of the specialty magnetic alloys which are manufactured have been evaluated at Perkin-Elmer. When the various desired properties - saturation flux density, permeability, magnetic hysteresis, and machinability - are traded off, the choice is narrowed down considerably. For instance, several of the alloys are formulated to be free machining, but can support only about 12,000 gauss. Several alloys have very high permeabilities, but are also limited by a low flux density capability. For this application, the design requirements of high force and small volume dictate a very high flux density, and since the gap is significant, the permeability is not critical, since the total path reluctance is determined by the gap.

The alloy which has been chosen as most suitable for this application is Hyperco-50, a soft iron manufactured by Carpenter Steel Corporation. Hyperco-50 is available in billets, and can be machined into the desired form factor. The techniques for machining and subsequently heat treating this material in order to obtain the desired properties have been intensively studied at Perkin-Elmer, and a number of magnetic devices have previously been manufactured on a prototype basis.

In order to obtain the optimum magnetic properties, the material must first be machined to form, and the unit assembled. The machining is performed at precisely controlled feed rates and speeds. In its raw form the material tends to be brittle, and care must be taken to ensure that the tool does not leave the material after a cut has been started. Additionally, only certain lubricating oils can be used for the machining process, and the material must be degreased immediately after machining. The material is then heat treated for a precise time interval in a hydrogen oven at 1825^{O}F, followed by a controlled cooling cycle. After the material has cooled completely, the distortion introduced by the heat treating is measured, and the critical surfaces are ground back to shape. The magnetic properties have been established by the thermal history, and very high temperatures or mechanical stress will disturb these properties.

Our experience with these alloys indicates that at least 23,000 gauss can be realized across the gap. The device design assumes a flux density of 20,000 gauss, and there are several other materials which are capable of this level of performance. These materials could be used if an alternative were required.

1.3-2 MAGNETIC CIRCUIT DESIGN

A traction motor which meets the basic parameters can be configured as follows, where the force is given by Equation 1.

$$F = \frac{AB^2 \times 10^{-6}}{11.8}$$

The device has been constructed from Carpenter Steel Hyperco-50, and a flux density of at least 20 kilogauss should be achievable with proper heat treating. The derivation of parameters will assume 20 kilogauss as a very safe number. The total gap area required is therefore:

$$A = \frac{(11.8)(100)}{400} = 2.795 cm^2 = 0.433 in^2 \qquad (3)$$

The total tractive area is nominally divided equally between the center post and the rim. The center post will have a 1/8 inch hole for the push rod, and the OD is given by:

$$\frac{\pi}{4}(OD^2 - (1/8)^2) = \frac{0.433}{2} \qquad (4)$$

$$OD = 0.54 \text{ in.}$$

Since the rim outer diameter will be 1.0 inch, the inner diameter is given by:

$$\frac{\pi}{4}(1.0^2 - ID^2) = \frac{0.433}{2} \qquad (5)$$

$$ID = 0.85 \text{ in.}$$

Allowing for a 15% flux leakage, as indicated by previous simulation results, the taper should be about 15%. Therefore, the outer wall will taper from 1.0 inch to 1.15 inch and will be sleeved appropriately. The inner post will taper from 0.54 inch to 0.60 inch.

Another tradeoff to be made is length. As the length is increased, the flux leakage is increased accordingly. However, as the length is increased, more wire can be wound, and the power dissipation decreases directly as the total amount of copper increases. An initial investigation which is partly intuitive indicates that an optimum length is between two and three inches. This investigation is the result of a quantitative look at the device simulation

and additional analysis is called for in this area. This analysis, however, is beyond the scope of this program. A length of three inches was chosen.

In addition, there are several geometry refinements which appear to be appropriate and which were incorporated. First, the corners were rounded instead of left sharp. Second, the armature was cut out so that the face of the armature matched the base profile at the gap. A sketch of the cross section of the device is shown in Figure 2.

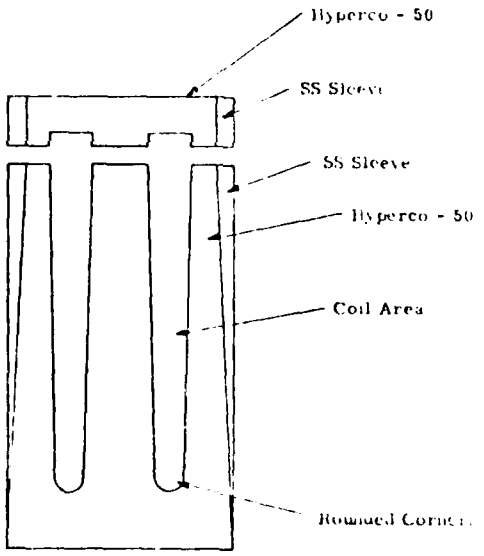

Figure 2. Cross Section of Electromagnetic Actuator

1.3-3 SPRING/FLEXURE DESIGN

In addition to the magnetic circuit, the actuator incorporates a spring configuration which has two main purposes. The first is to support the armature or moving portion of the actuator to the base. The second is to maintain a precisely controlled spring constant. Again, machinability is an issue, and the spring material must have a very low mechanical hysteresis within the precision elastic limit. Tensile strength should be high, and Young's modulus very predictable. Naturally, the material must be non-magnetic so as not to interfere with the operation of the magnetic circuit.

The only material which can seriously be considered is beryllium-copper. A study of the various applicable alloys indicates that KBI* alloy 172 offers the required properties. Alloy 172 comes in two forms designated by manufacturers as Condition A and Condition H. Condition A is annealed and soft, permitting bending to shape. Condition H is partially hardened and suitable for machining operations which do not require bending. Both types have the same Young's modulus when heat treated, but the Condition H material cures to a higher tensile strength.

The machining and heat treating of these alloys are well understood. The material is first machined to the desired form, heat treated in a fixture, and the heat treatment is checked by measuring the hardness of the material. Measured spring constants generally check with calculated values very well.

1.3-4 COIL/DRIVE AMPLIFIER

In order to generate the magnetic flux, the unit contains a drive coil wound around the center pole. This coil is interfaced with a power amplifier. The designs for both the coil and the amplifier are very closely related. The total drive requirement is determined by the wire area and the current density. The drive is specified in ampere-turns. The coil can be configured either from a large number of turns of fine wire, or from a lesser number of turns of heavier wire. As the number of turns increases, the current decreases, but the inductance of the coil increases as the square of the number of turns. This subsequently increases the voltage requirement of the amplifier.

The amplifier should be a true current amplifier, that is, it should drive the coil with a constant current proportional to the amplifier input voltage. The limitation on the amplifier design is that suitable power trans-

* Karwacki Beryllium, Inc.

istors perform best at output currents less than 8 amperes. Since the drive requirements for this unit are not severe, it seems that a 3-ampere coil will meet all the salient performance requirements and will be reasonable to manufacture.

There are two ways to realize a device with suitable characteristics. The first way is to drive the actuator coil with an ordinary feedback voltage amplifier, and to ground the coil through a small, stable resistor. The resistor voltage is now proportional to the coil current, and this voltage can be used to derive negative feedback for gain stabilization. This technique has the advantage that the gain is extremely stable (as stable as the feedback resistor), and the disadvantage of requiring a feedback loop which may tend to be oscillatory as the coil inductance varies due to non-linearities.

A second way to construct a current amplifier is to use a single power transistor with a large emitter resistor in the output stage, and place the actuator coil in series with the collector. The collector current is approximately equal to the emitter current, which is determined by the base voltage. That is, the impedance looking into the base is equal to the transistor β times the emitter resistance. This can be seen to be considerably simpler than the first approach and is the technique which is generally used in TV flyback amplifier circuits.

Figure 3 is a simplified schematic of an amplifier capable of supplying from 0 to 6 amperes to an electromagnetic actuator. The amplifier controls the current through the actuator, and allows the voltage across the actuator to change by ±10V as necessary. The amplifier gain will be adjusted so that an input range of - 10 volts to + 10 volts will correspond to zero to full deflection.

Transistors Q1 and Q2 are connected in such a manner that $I_A = \alpha I_E$, where $0.995 < \alpha < 1.000$. (refer to Figure 3). Thus, to a very good approximation,

$$I_A = -(A_1 V_{IN} + A_2 V_{BIAS}) \qquad (6)$$

Diode D1 and Zener diode D2 protect Q1 and Q2 from damage if an input that causes I_A to decrease rapidly is applied to the amplifier.

Q2 and D2 can dissipate as much as 40 watts of power at full current output. A 2 in. x 4 in. x 6 in. convection-cooled heat sink is necessary to keep Q2 and D2 within safe temperature limits. The remaining components are mounted

on a 3 in. x 5 in. circuit board. The prototype amplifier weighs about 1 pound, and the goal for a final design would be several ounces.

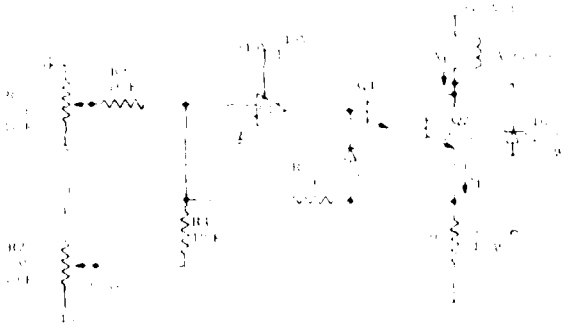

Figure 3. Drive Amplifier Simplified Schematic

1.3-5 *PUSH ROD ANALYSIS/DESIGN*

The linkage between the magnetic actuator and the mirror consists of an axial length adjustment assembly, a push rod, and a spring. Of these components the push rod is most critical, warranting consideration of both natural frequencies and buckling loads. A preliminary sketch of the proposed device is shown in Figure 4.

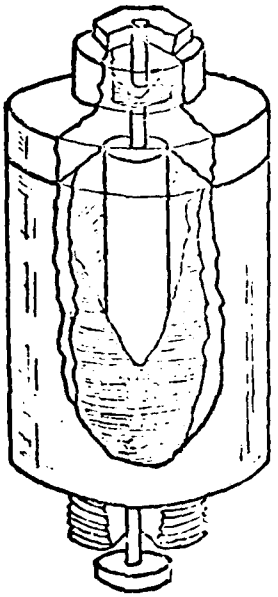

Figure 4. Electromagnetic Actuator Conceptual Drawing

Three modes of vibration are possible: longitudinal, torsional, and transverse (bending). The first two modes can be eliminated from this analysis. The longitudinal vibration has a small amplitude with a high natural frequency (over 10kHz), and torsional vibration does not significantly affect performance. However, the transverse vibration occurs at a natural frequency close enough to the operating frequency to require provision in the design to avoid resonance problems.

The push rod was considered as a "clamped-hinged" beam (Figure 5) for which the following formula for transverse vibration is applicable.

$$f_n = \frac{15.4}{2\pi} \sqrt{\frac{EI}{\mu \ell^4}} \qquad (1)$$

where

f_n = Natural frequency

EI = Bending stiffness of the section

ℓ = Length of the beam

μ = Mass per unit length

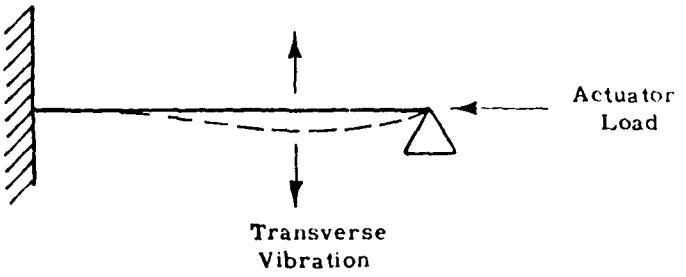

Figure 5. Mechanical Model of Push Rod

When slender members are loaded in compression, they tend to buckle and experience significant lateral deflections that are functions of the applied loads. Computations were performed using empirical column data for various values of push rod diameter and modulus of elasticity. The same ranges of diameter and modulus of elasticity were applied in computations of natural frequency. The results of these computations for cylindrical section push rods are presented in Figure 6. Three major design requirements can be identified; the rod must be non-magnetic, the natural frequency must exceed 1400 Hz, and the allowable compressive working load must exceed 80 pounds. There are numerous alternatives for the push rod design. For example, a brass ($E = 20 \times 10^6$ lbf/in.^{2}) rod with a diameter of 0.135 in. could be employed. However, it is advantageous for the rod to be thin. Consequently, a design study will select a suitable material and perhaps a non-cylindrical cross section.

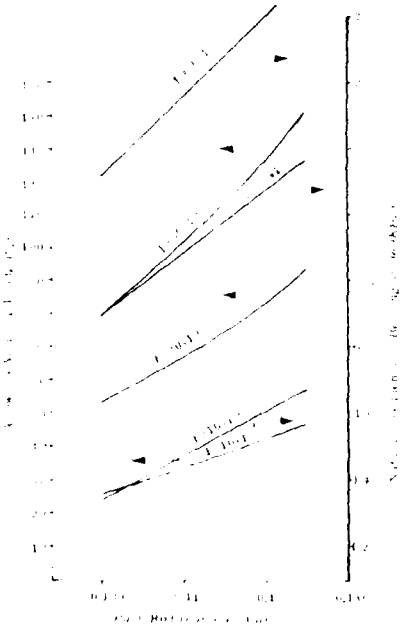

Figure 6. Push Rod Allowable Load and Natural Frequency

1.4 DEVICE NONLINEARITIES

One of the salient characteristics of this type of device is that the force is proportional to the flux density squared, and therefore to current squared. This is made even more severe when it is noted that the force is also inversely proportional to the gap, and therefore, if the total stroke is not insignificant with respect to the gap, the force may be proportional to an even higher power of the drive current.

There are several factors which tend to moderate the effects of this nonlinearity. In actual practice, the permeability of the magnetic material decreases as the flux density increases, and it is possible to configure a unit so that the permeability variation compensates for the squaring factor. That is, the flux density becomes proportional to the square root of the drive current in the operating regions of interest. In actual practice, we have plotted very nearly linear force vs. current characteristics with linear spring. The nonlinearity due to a large stroke should not exist, since, for the device being considered, the stroke will be small compared to the initial gap.

A further consideration is the inherent instability of the device. For a linear spring/flexure constant, as the current is increased, the force pulls the armature closer to the pole structure. This situation becomes analogous to moving a permanent magnet closer and closer to a piece of iron. At the critical position, the iron suddenly jumps to the magnet. For our actuator, there is a critical value of current at which the armature is pulled to the pole. In the solution of the two equations which govern the behavior of the device, this is the point at which less current is required to maintain a greater deflection. We have generated a simulation to predict this behavior as a function of coil parameters, spring deflection parameters, initial gap, device geometry, and drive current. The result of the runs which we have made, on devices very similar to this device, is that the instability occurs at a deflection of about 1/3 of the initial gap. It is possible to adjust the initial gap so that this phenomenon will not be a problem. A stop is installed in order to prevent an unstable condition from occurring and damaging the spring or the deformable mirror.

1.5 THERMAL CONSIDERATIONS

One of the critical factors to be considered is the thermal expansion of the actuator due both to heat generated in the coil and to eddy currents in the magnetic circuit. The effects of thermal expansion are mitigated by the fact that the magnetic circuit expands in one direction, and the push rod expands in the opposite direction. Ideally, the push rod should have an expansion coefficient equal to that of Hyperco-50 (about 6×10^{-6} in/in/°F). The one material that stands out as having a high E and the right expansion coefficient is Beryllium. Unfortunately, beryllium cannot be routinely machined due to toxicity considerations, and if a push rod were fabricated, it would not be possible to make any required adjustments to the dimensions in-house. Therefore, the initial push rod was fabricated from tungsten which has a much lower expansion coefficient. Beryllium is considered as suitable for a later effort, after the more basic design considerations have been resolved. (A second push rod was fabricated from stainless steel, after the tungsten rod cracked due to brittleness.)

1.6 PEAK DISPLACEMENT CONSIDERATIONS

The maximum allowable displacement is a function of the spring mechanism and the initial air gap between the base and the armature. For the peak-to-peak motion of 31.8μm, the spring is essentially linear, and the devices of this type have been found to be unstable for displacements of about 1/2 of the initial gap. Since the power requirements will increase as the square of the gap, it is desirable to keep the initial gap as small as possible. The gap will be set at about 0.003 in. = 7.62×10^{-3} cm. The gap is initially adjusted to be uniform with a toolmaker's microscope, and can be set to within ±10%. The maximum displacement will be set by fastening metal stops in the gap.

1.7 ACTUATOR RESONANCES AND NATURAL FREQUENCY

There are two mechanical resonances of interest. The first is the resonance due to the armature on the spring. This resonance is given by

$$f = \frac{1}{2\pi} \sqrt{\frac{K}{M}} \qquad (8)$$

where K = spring constant (lb/ft)

M = mass (slugs)

For a typical spring on the device pictured in Figure 5, we have measured a displacement of 0.0015 inch for a force of 83 pounds. Therefore:

$$K = \frac{83 \times 12}{0.0015} = 6.64 \times 10^{5} \text{ lb/ft} \qquad (9)$$

The mass of the armature is

$$\frac{0.26 \text{in}^3 \times 2.285 \text{ lb/in}^3}{32} = 2.32 \times 10^{-3} \text{ slug} \qquad (10)$$

and: $$f = 2{,}693 \text{ Hz} \qquad (11)$$

This may be lowered slightly by the mass of the push rod. The second resonance is caused by the transverse vibration of the push rod. The push rod will be 0.1 inch diameter, and will be made of a tungsten alloy with E = 4×10^{7}. It can be seen, from Figure 6, that the natural frequency of the rod is greater than 2.8 kHz. We do not envision any problems in meeting the 800 Hz resonance limitation requirement.

II. FABRICATION

2.1 MACHINING PROCESSES

The pieces of the actuator were fabricated as per drawings 687-2064 to 687-2073 which are included as Appendix A. The machining procedures used are as follows:

1. **Post-Center** (687-2064)
   The center post was turned to form from Carpenter Steel Hyperco-50.
2. Cap (687-2065)
   The cap was turned and threaded from 303 stainless steel.
3. Case (687-2066)
   The case is designed to fit over the base and is turned from 303 stainless steel. It is fastened to the base with Loctite 35 retaining compound.
4. Post - Threaded (687-2067)
   The post is configured to mate the actuator test cell. It, also, is machined from 303 stainless steel, and the threads are turned on a lathe. It is fastened to the base with Loctite 35.
5. Nut - Differential Adjust (687-2068)
   The differential nut is turned from 303 stainless steel. The metric and American Standard Threads are accomplished by changing the back gears on the lathe.
6. Armature (687-2069)
   The armature is turned from Hyperco-50, and is configured to match the center pin.
7. Flexure (687-2070)
   The spring flexure is machined from BeCu - Alloy 172, and subsequently annealed.
8. Spring (687-2071)
   The spring is machined from BeCu - Alloy 172 and annealed. The thickness was selected experimentally, and is 0.027 inches.
9. Base (687-2072)
   The base is turned from Carpenter Steel Hyperco-50 and the center pin was press fitted to the center hole.
10. Adj - Push Rod (687-2073)
    The push rod was fabricated from a length of solid tungsten. The threaded portions were made on 303 stainless steel sleeves which were heated and shrunk onto the tungsten rod.

2.2 COIL

The coil was wound from #24 double formvar insulated wire on a delrin form configured to match the actuator form factor. After several iterations, we selected a coil with 410 turns total. The coil was potted, one layer at a time, and pressed into the actuator. The fit is very tight, and it cannot be removed intact.

2.3 ASSEMBLY

The electromagnetic actuator was assembled in accordance with layout drawing 687-10086 shown in Appendix A. First, the center pin was press fitted into the base. The cap and case were then degreased and secured to the armature and the base with loctite retaining compound 35. Both assemblies then required holes to be drilled at the joint between the stainless steel and the Hyperco-50. This was done in a jig boring machine. The loctite joints were then broken, by heating the assemblies in an oven to 800^{O}F, and the bottom assembly, along with the armature, was sent to Carpenter Steel for the proper conditioning and heat treating, to generate optimum magnetic properties. The cap and case were then refastened, and the 2-56 holes tapped in both.

After a one week settling period, during which the Hyperco-50 tended to settle, both gap surfaces were ground flat, and the device was assembled. The gap is set at 0.0042 inch by using a toolmaker's microscope, and the special tool which is supplied. Three stops, which limit armature travel to 0.0012 inches were inserted into the cap at a later time.

The major actuator components are shown in Figure 7, and the assembled actuator is shown in Figures 8 and 9.

2.4 ELECTRONICS

The objectives of the amplifier design phase were to construct an amplifier which could be used to drive the actuator for proof of principal, and to demonstrate that a very small and efficient amplifier was feasible. The approach taken was to design and build a linear amplifier to use for test purposes, and to design a switching amplifier as a parallel effort. The class B linear amplifier should have an efficiency of about 50%, compared to better than 90% for the switching device.

2.4-1 CLASS B LINEAR AMPLIFIER

The amplifier schematic is shown in Figure 10. The design employs current feedback from resistors R10 (.2 Ω) and R4(1KΩ) back to the low power level 747


CM 1 2 3 4 5

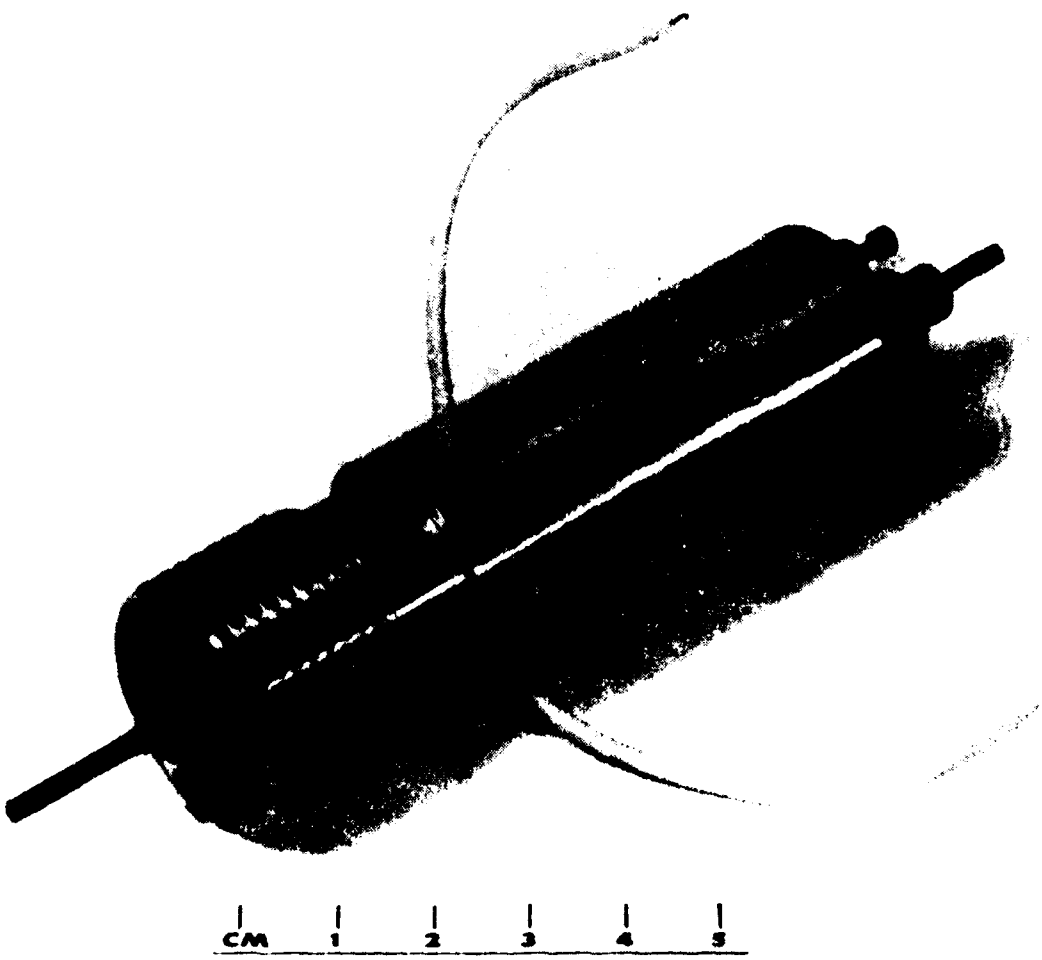
CM
1
2
3
4
5

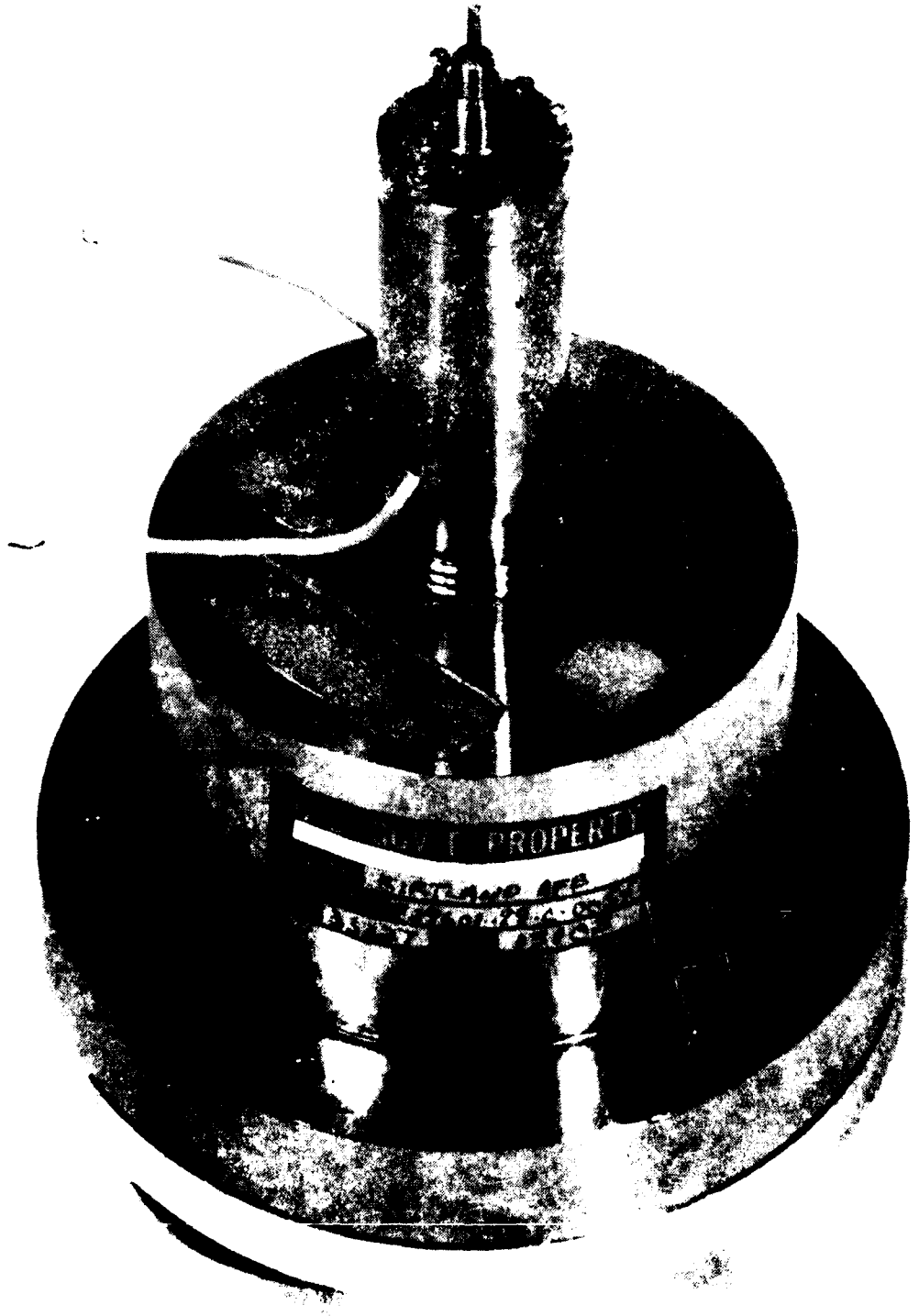

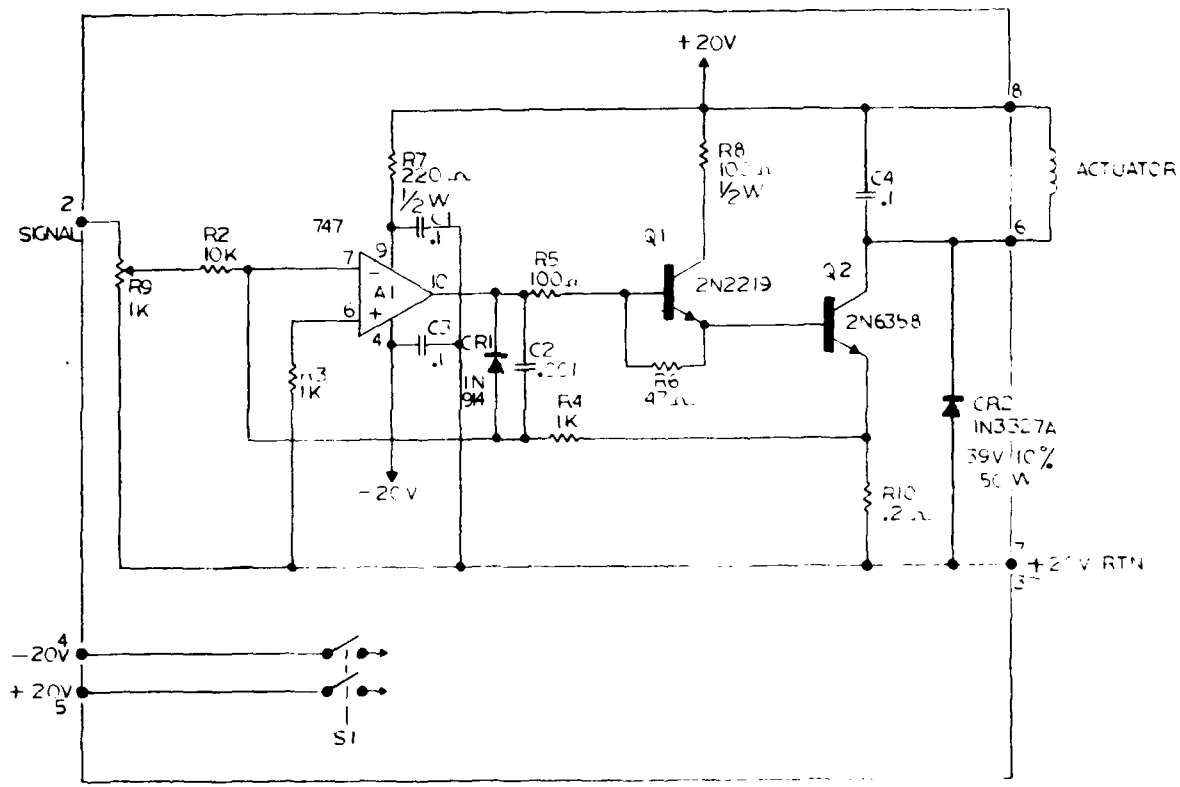

CLASS B AMPLIFIER

Figure 10. Schematic of Class B Linear Amplifier

op-amp. (A1). The 747 output drives the cascaded Darlington transistor Q_1 (2N2219) and Q_2 (2N6258). The latter output transistor drives the actuator, while zener diode CR2 (1N3827A) provides voltage protection for the collector junction of Q_2. The breadboard amplifier is illustrated in Figure 11.

2.4-2 SWITCHING AMPLIFIER

To reduce size, weight, and power consumption a switching amplifier design was undertaken. It is shown schematically in Figure 12.

The goal of high efficiency is achieved by operating the Unitrode PEC633 Darlington power device in either full ON or full OFF mode, with the duty cycle establishing the average power. The actuator's natural inductance filters the switching carrier current to an acceptable amount. The duty cycle is controlled by comparing the command input or control voltage to a triangle input. With the control at zero, the offset potentiometer R2 is adjusted until the comparator provides a 10% duty cycle square wave to the output power device. As the control voltage increases positively the duty cycle increases linearly until a maximum of nearly 100% or full on is obtained. The switching amplifier breadboard is shown in Figure 13.

2.5 SPECIAL TOOLING

The following tools, illustrated in Figure 14, were fabricated as aids in assembling, aligning and installing the actuator. The small wrench in the lower center is used to loosen and tighten the nuts to adjust the gap. The long thin device in the upper right engages the coarse and fine preload adjustments, and the large tool on the left is used to turn the actuator into the mirror.

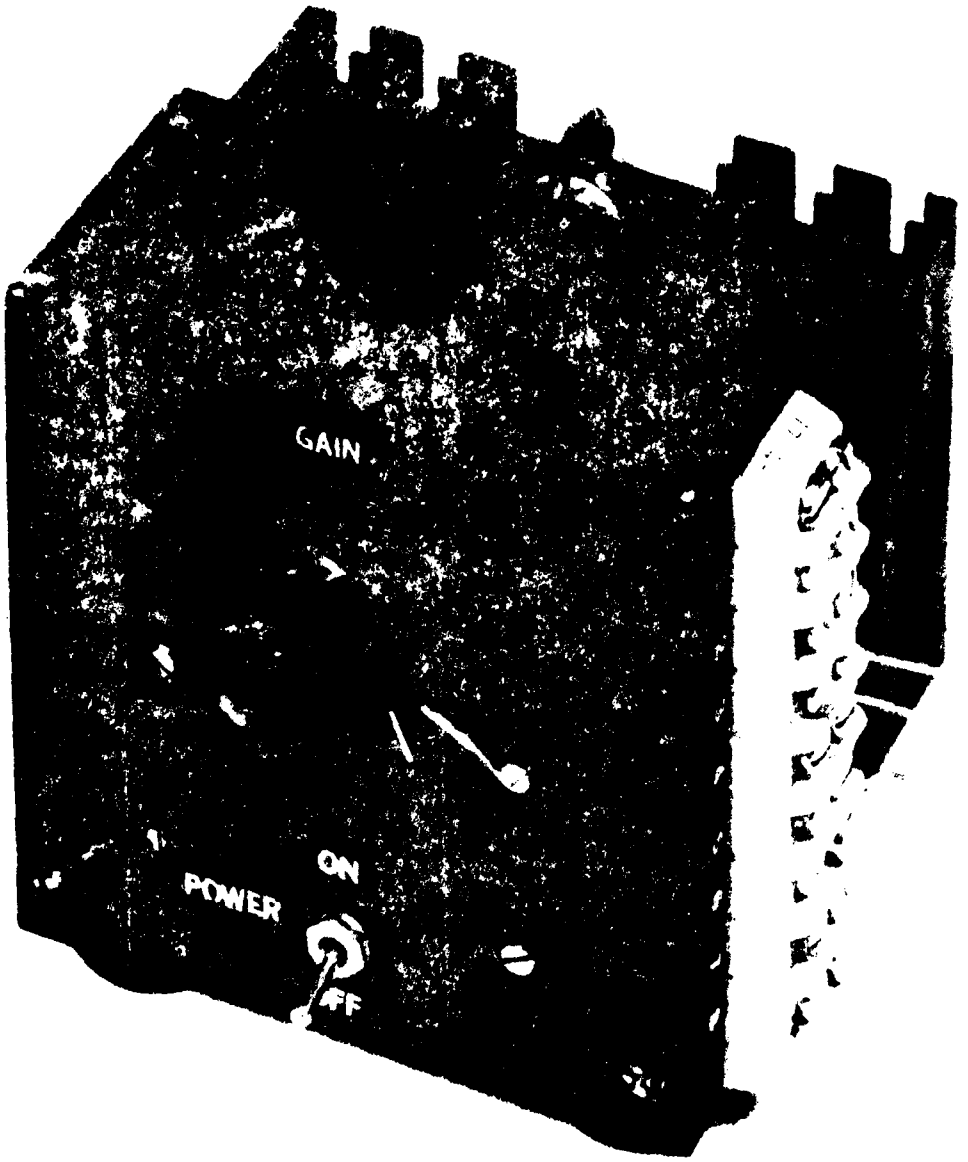
GAIN
POWER
ON
OFF

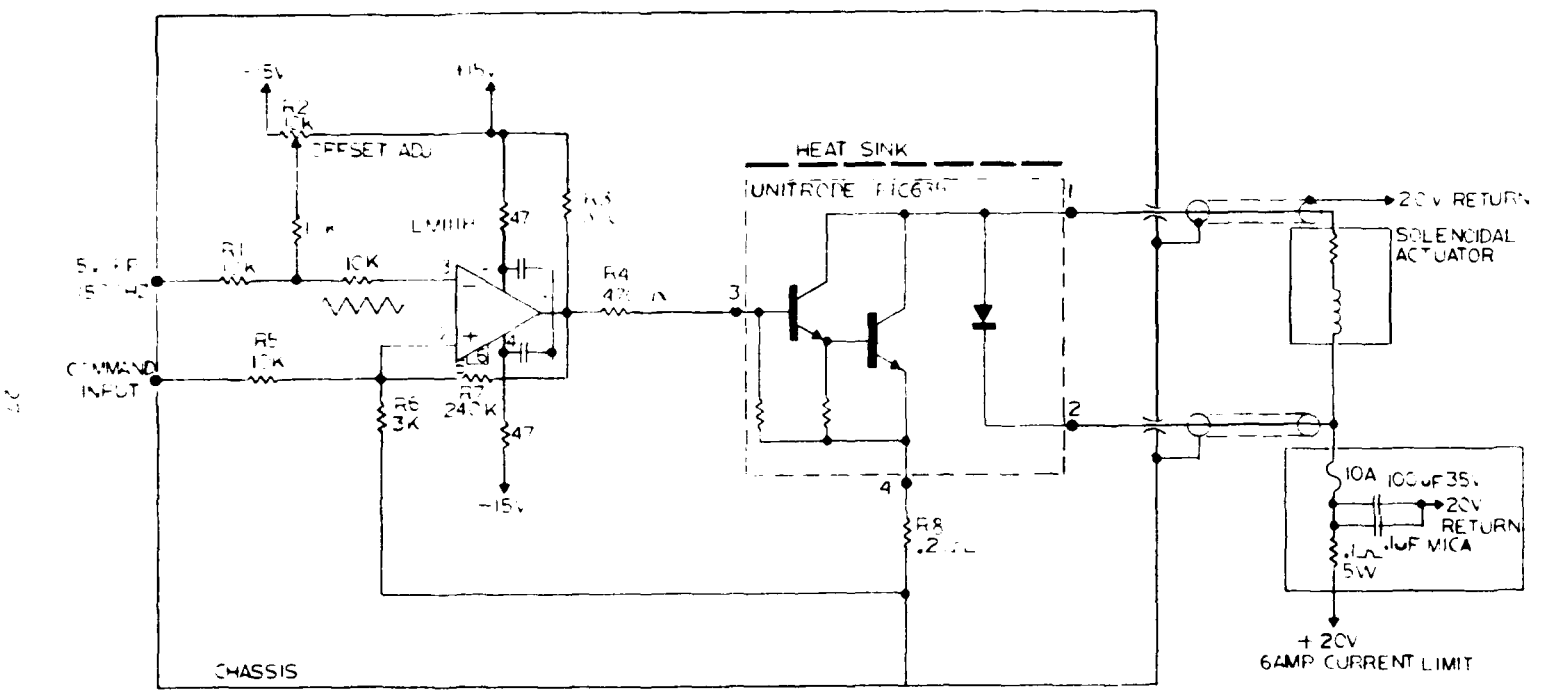

SWITCHING AMPLIFER

Figure 12. Schematic of Switching Amplifier

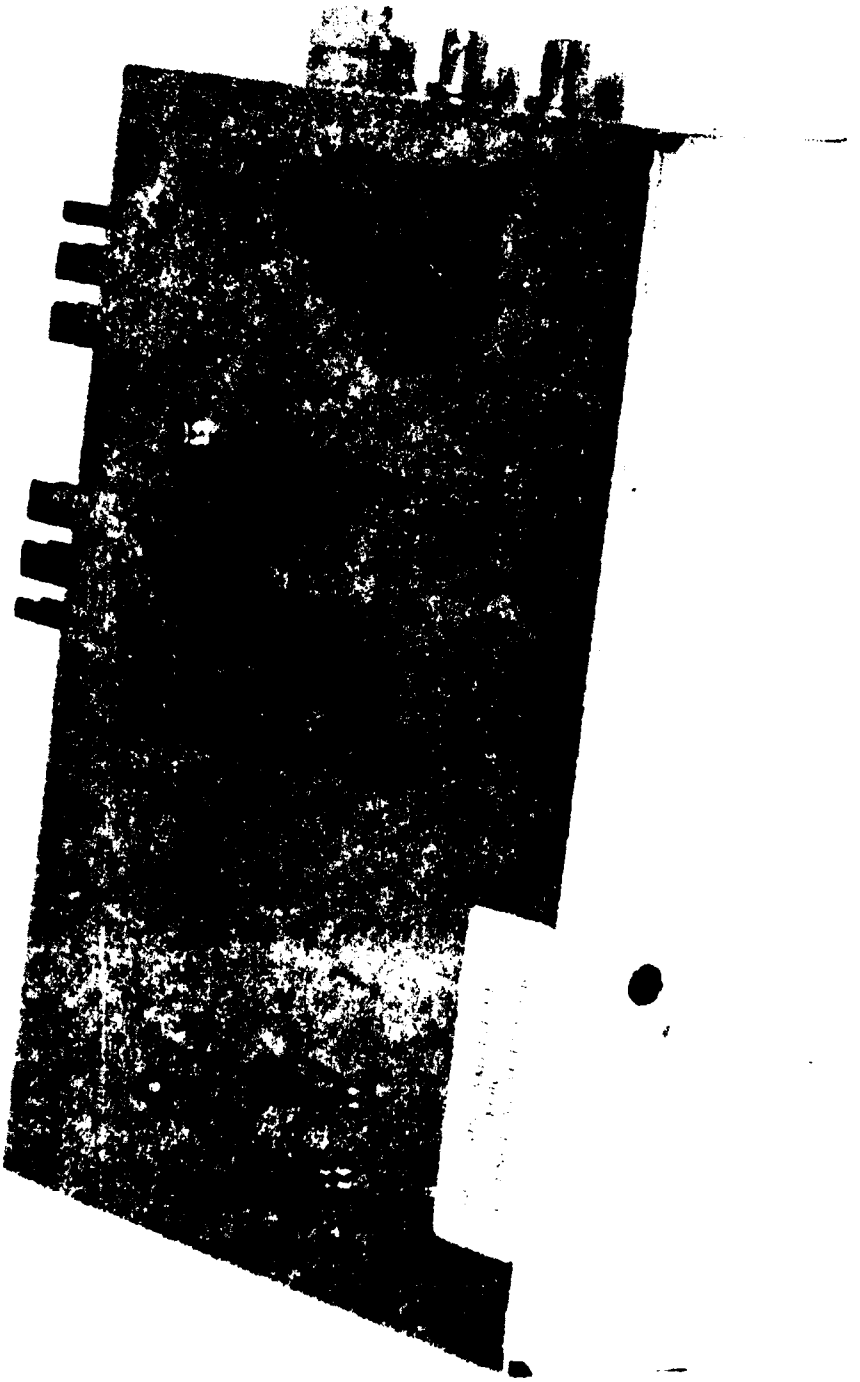

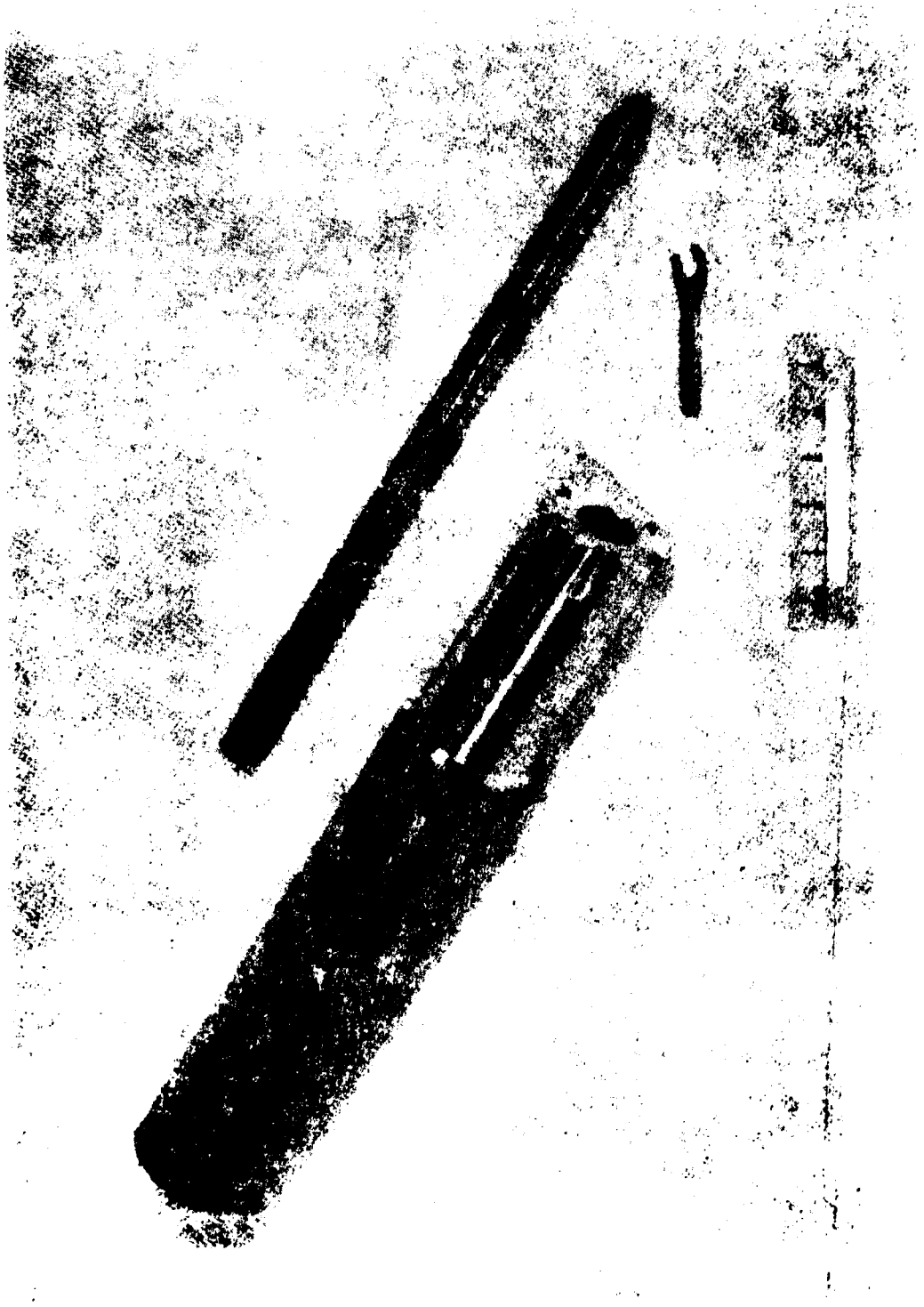

III. TEST PROCEDURE AND RESULTS

3.1 MIRROR CELL TESTS

The first test performed was a displacement/force measurement in order to determine exactly how much force was necessary to displace the mirror. A billet of material was machined, which fit into the test cell, and has a recess which meshed with the nipple on the simulated mirror surface. A calibrated force gage was used to push on this billet, and the displacement at the billet was measured with a dial indicator. It was determined that a force of 60 pounds deflected the test cell surface the required 1.2×10^{-3} inches.

3.2 ACTUATOR FORCE TEST

The initial test on the assembled actuator included displacement, and force measurements. The maximum available force is determined by first calibrating a relatively thick spring, by measuring its displacement due to a known force, and the displacement as a function of current.

Our tests were first made without the push rod installed, and a 0.078 inch spring which had previously been made was used. This was the thickest BeCu spring which we had available. The actuator was assembled and aligned with a gap of 0.0032 inches, and it was determined that the spring constant was 78,260 lb/inch. Current was then applied, and the highest stable displacement obtainable was 1.55×10^{-3} inches, for a current of 1 ampere.

$$78{,}260 \text{ lb/in} \times 1.55 \times 10^{-3} \text{ in} = 121 \text{ lb} \qquad (12)$$

This implies that the device was capable of 120 lb. It was not readily possible to determine if larger forces could be realized, since a thicker spring was not available. Also, this force is somewhat greater then we had anticipated, and is certainly very adequate.

We then determined the static positional hysteresis of the device by setting the excitation at 500 milliamperes, and varying the current so that we obtained this value of current by monotonically approaching from zero or one ampere. Using a B&S electronic dial indicator, we estimated that the hysteresis, again without the push rod, was between 7 and 25×10^{-6} inches - or 0.18 to .64 micrometers. This estimate is of questionable validity, since the spring is substantially thicker than the final spring, and it was very difficult to repeat the current accurately.

With the assurance that the actuator had ample force capability, the push rod was then installed, and the mirror test cell was used to simulate the actual mirror surface.

3.3 ELECTRICAL TESTING

Electrical tests were performed with both amplifiers with a dummy load. The dummy load was established from sinusoidal measurement of actuator impedance characteristics. The resulting model is shown in Figure 15.

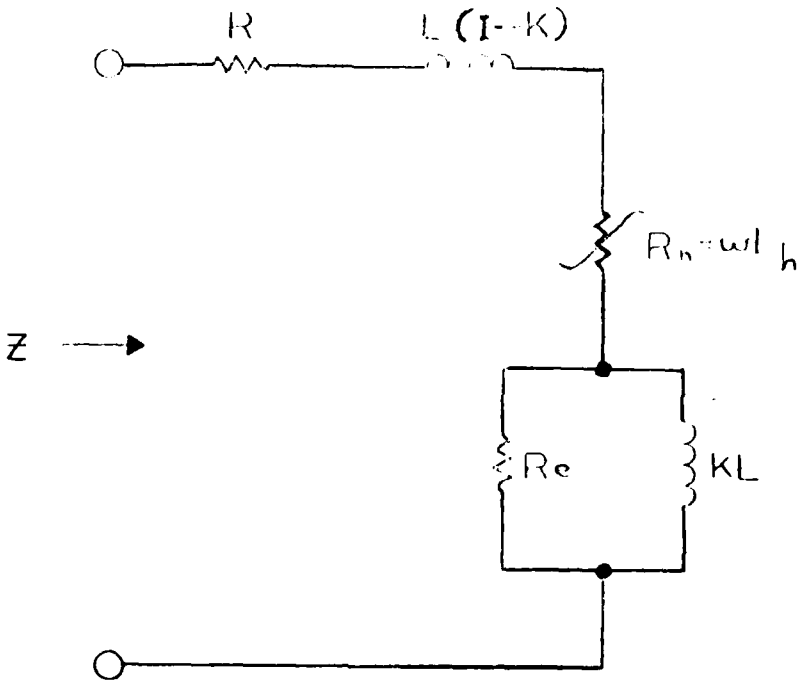

R = resistance due to copper losses (0.67 ohm)

L = open circuit inductance (12.7 mH)

L(1-K) = leakage inductance (0.38 mH)

KL = magnetizing inductance (12.3 mH)

L_h = hysteresis inductance (.29 mH)

R_e = resistance due to eddy currents (774 ohm)

Figure 15. Electrical Actuator Model

Static tests on both amplifiers were performed. DC actuator current versus input voltage was measured and resulted in the plots in Figure 16. For the switching amplifier it is noted that one ampere of d.c. current prevails with no input. This is due to the bias and adjustment for a ten percent duty cycle. If the switching amplifier characteristic is translated down by one ampere it is obvious that this linearity is inferior to the class B amplifier.

The class B amplifier was tested dynamically with square wave and sinusoidal input waveforms. The square wave tests were performed from 10Hz to 1kHz with peak currents ranging from 0.25 amp to 3.5 amperes. Some of these results are shown in the oscilloscope traces of Figure 17. Frequency responses for both amplifiers are shown in Figure 18.

3.4 TEMPERATURE TESTS

The amplifier was environmentally temperature tested at maximum power and frequency. The actuator current was set at a peak current of 1.7 ampere using the class B amplifier at a frequency of 150Hz. The current stayed constant for $10^{O}F$ interval temperature rises up to $113^{O}F$ ($45^{O}C$). The maximum temperature of the actuator case reached $68^{O}C$ while the amplifier heat sink rose to $33^{O}C$ at room ambient ($27^{O}C$).

3.5 PERFORMANCE TESTS IN AFWL TEST CELL

The push rod was then installed in place, and the bottom flexure adjusted to a slight preload. The actuator was tightened into the test cell, and the tests were repeated. Full deflection of 1.2 millinches was noted with a drive current of 1.5 amperes, and the hysteresis was consistent with previous results. Quantitative data, however, was not taken due to the fact that the performance was noted to deteriorate shortly after the device was installed in the test cell. An examination of the device showed that the threads on the push rod were the mechanism for this deterioration, and it is believed that the higher than anticipated peak force was a contributing factor. When the flexures were loosened, the play in the push rod threads was several thousandths of an inch. Initially, we were able to compensate for this play by increasing the preload, but this finally resulted in greater deterioration. Finally, the stroke was limited to about 1/3 of the spec value.

3.6 TEST AT AFWL

The static tests were repeated at AFWL on 11 September, and a series of dynamic tests were run. At this time, the threads had deteriorated badly. Due

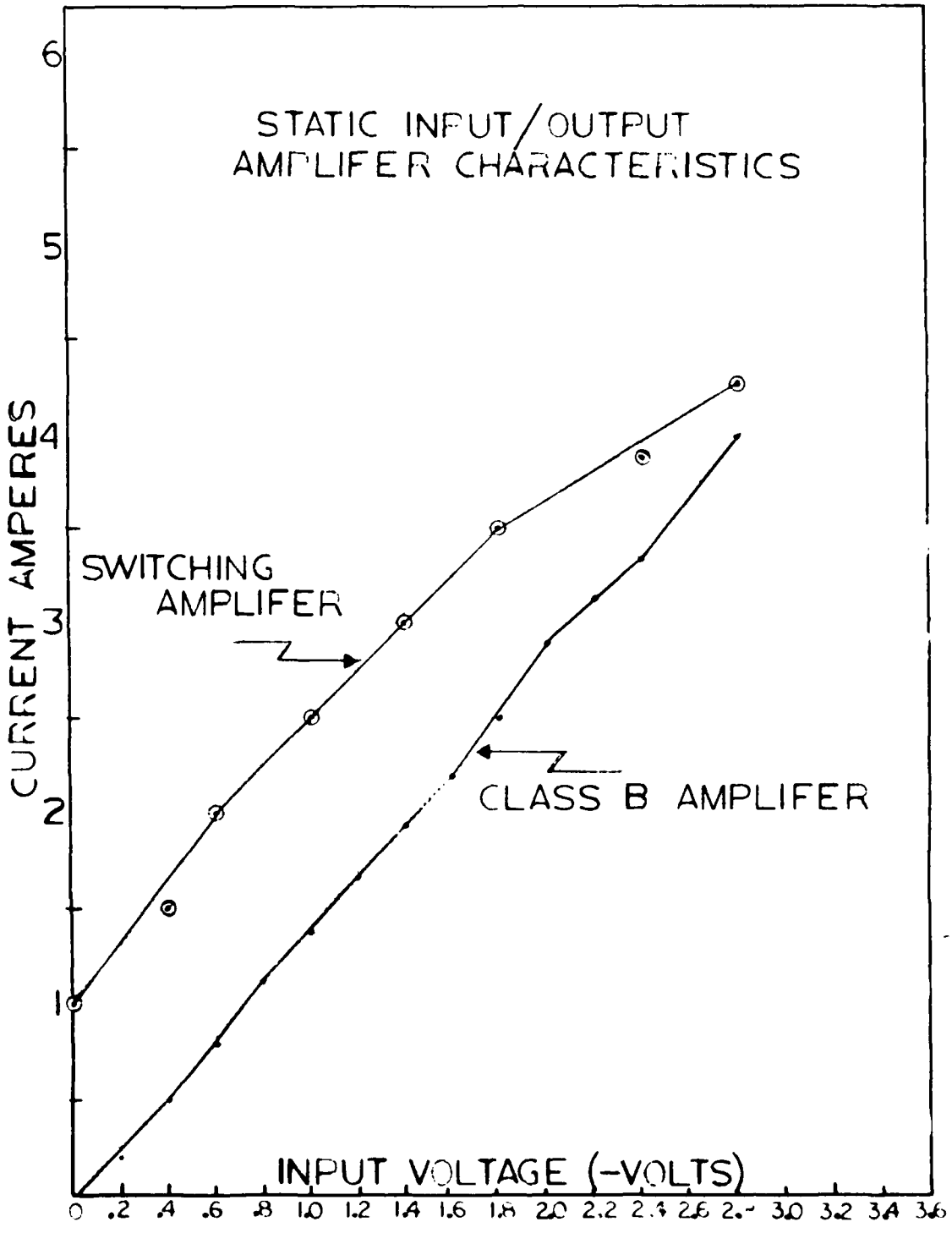

Figure 16. Static Input/Output Amplifier Characteristics

100 Hz,

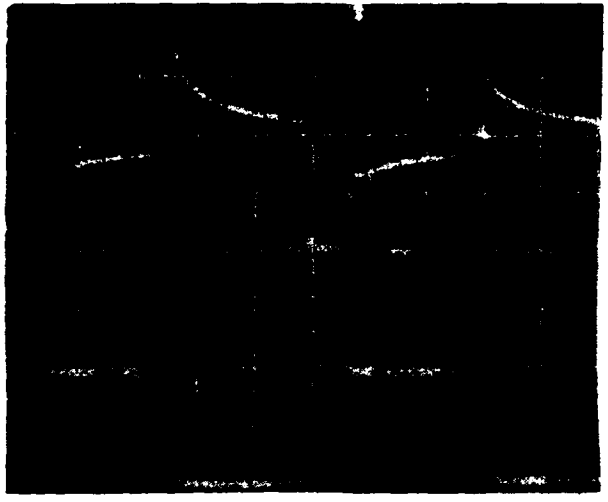

1 kHz,

1 kHz,

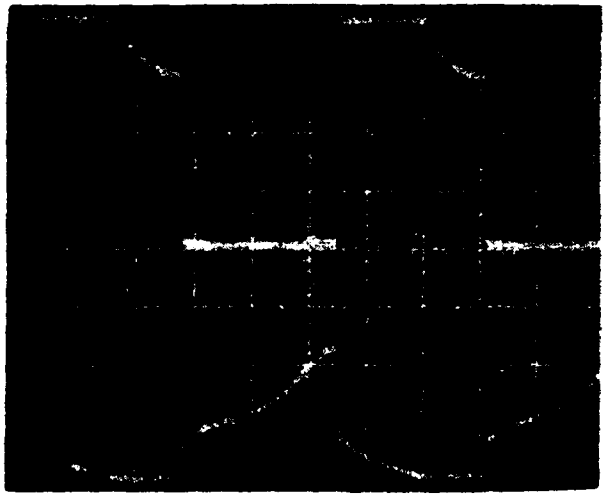

1 kHz,

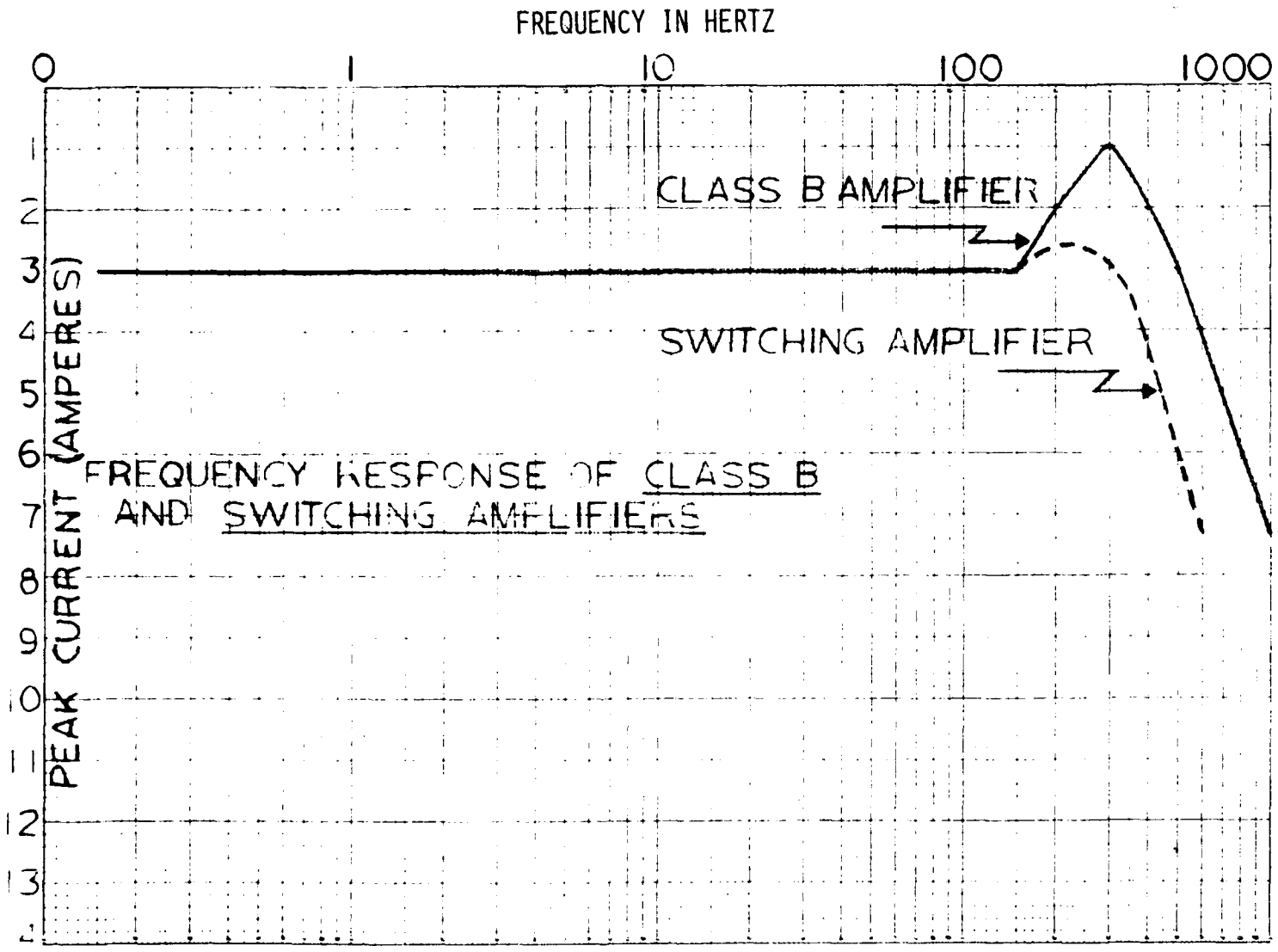

Figure 18. Frequency Responses for Both Drive Amplifiers

to this deterioration, the stroke was limited to about 10 micrometers. These data are available at AFWL. The threads were reworked, and the diameter increased subsequent to this deterioration, and retested at Perkin-Elmer. This retest indicates that a stroker greater than 14 micrometers is possible. The results of this retest are shown in Figure 19.

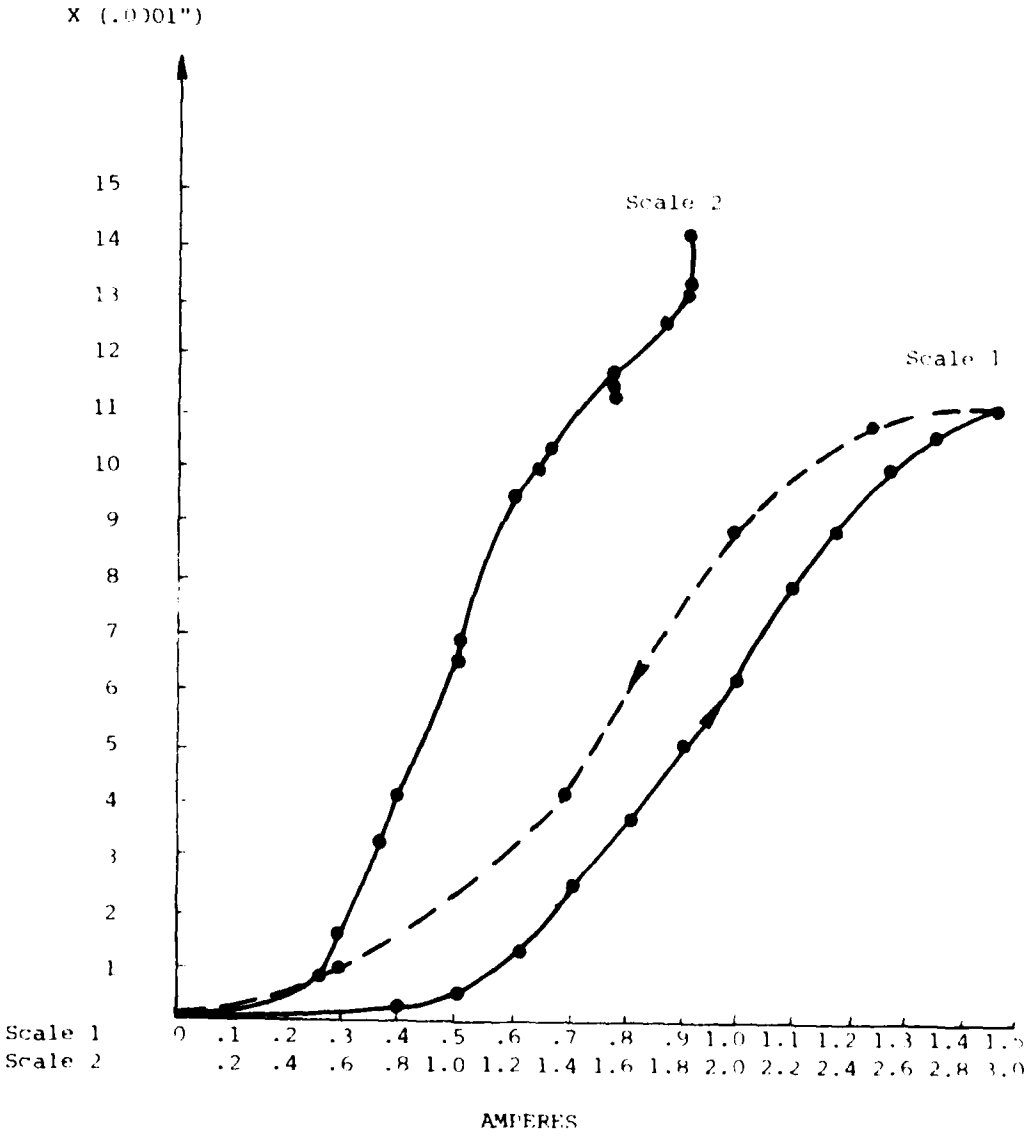

Figure 19. Static Displacement/Current After Thread Rework

APPENDIX A

Actuator Drawings

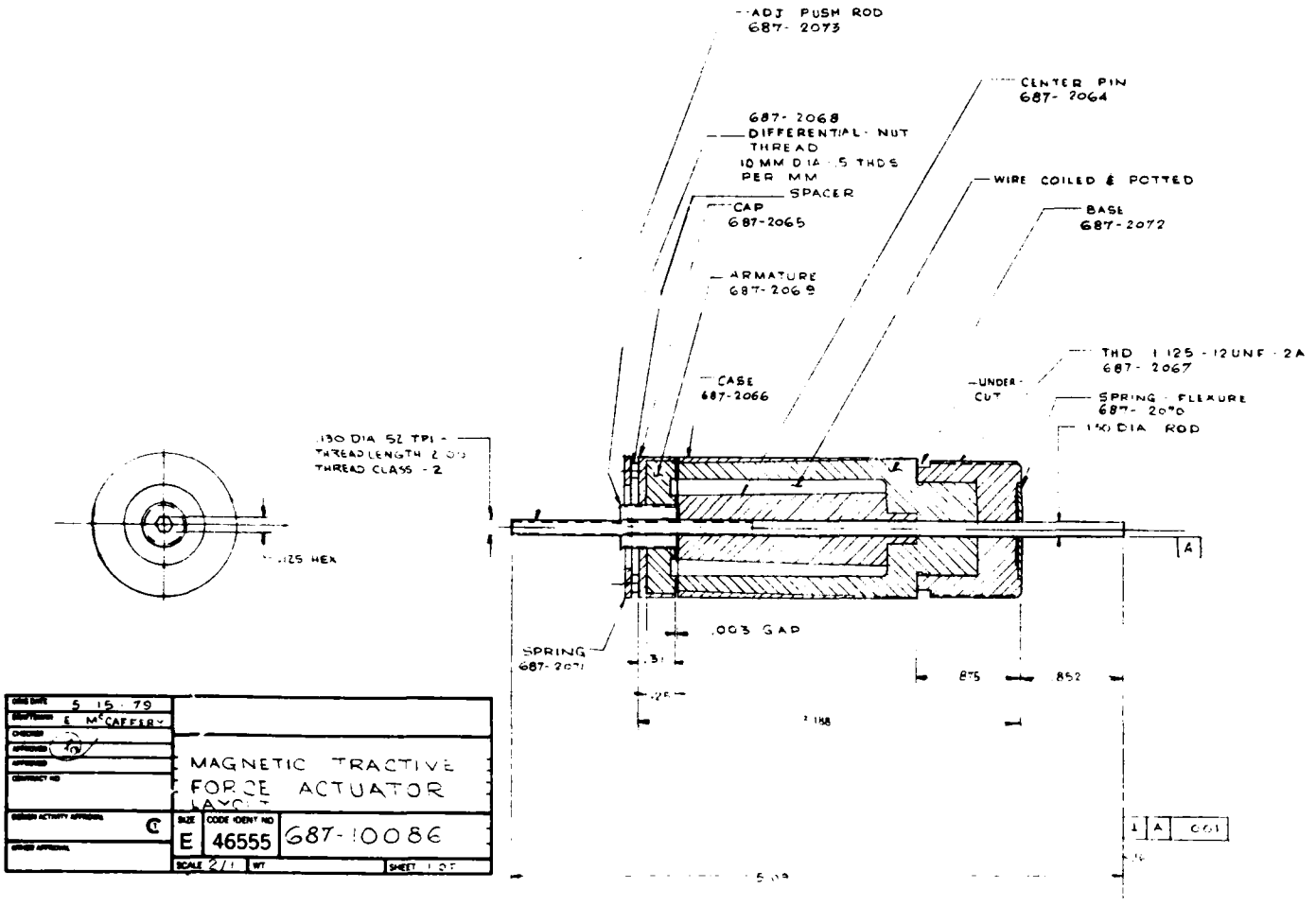

Figure A1. Magnetic Tractive Force Actuator Layout

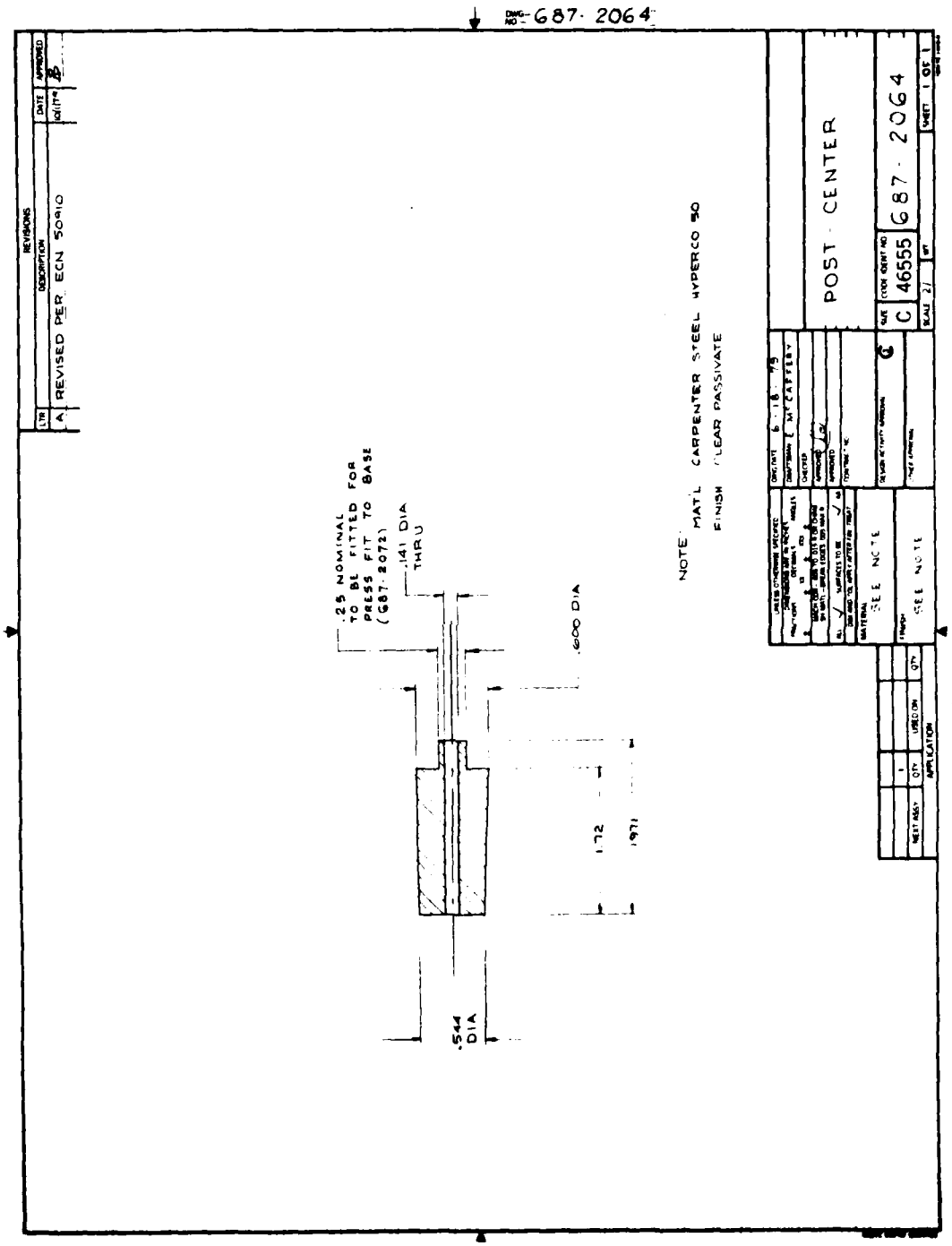

Figure A2. Post-Center

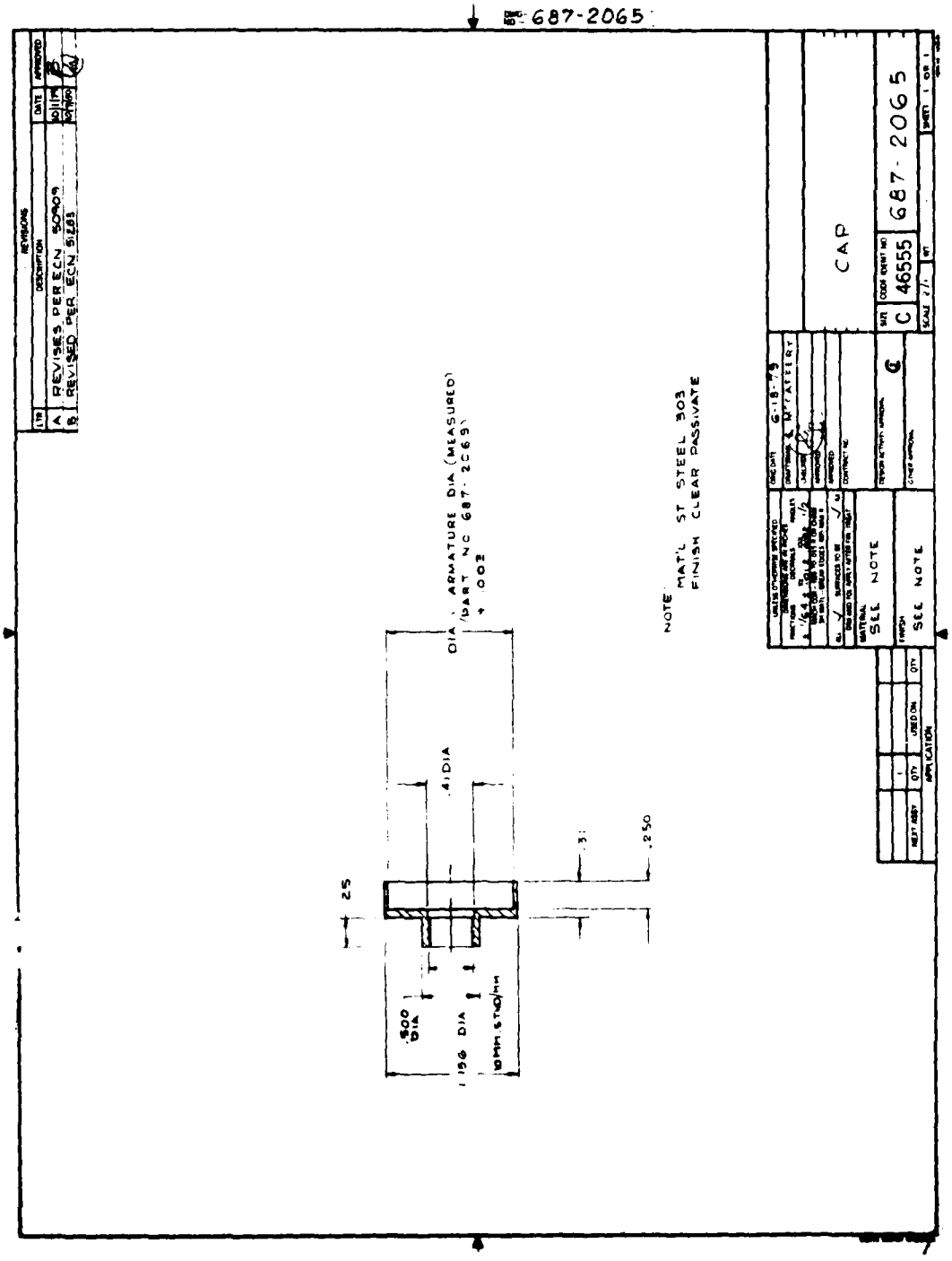

Figure A3. Cap

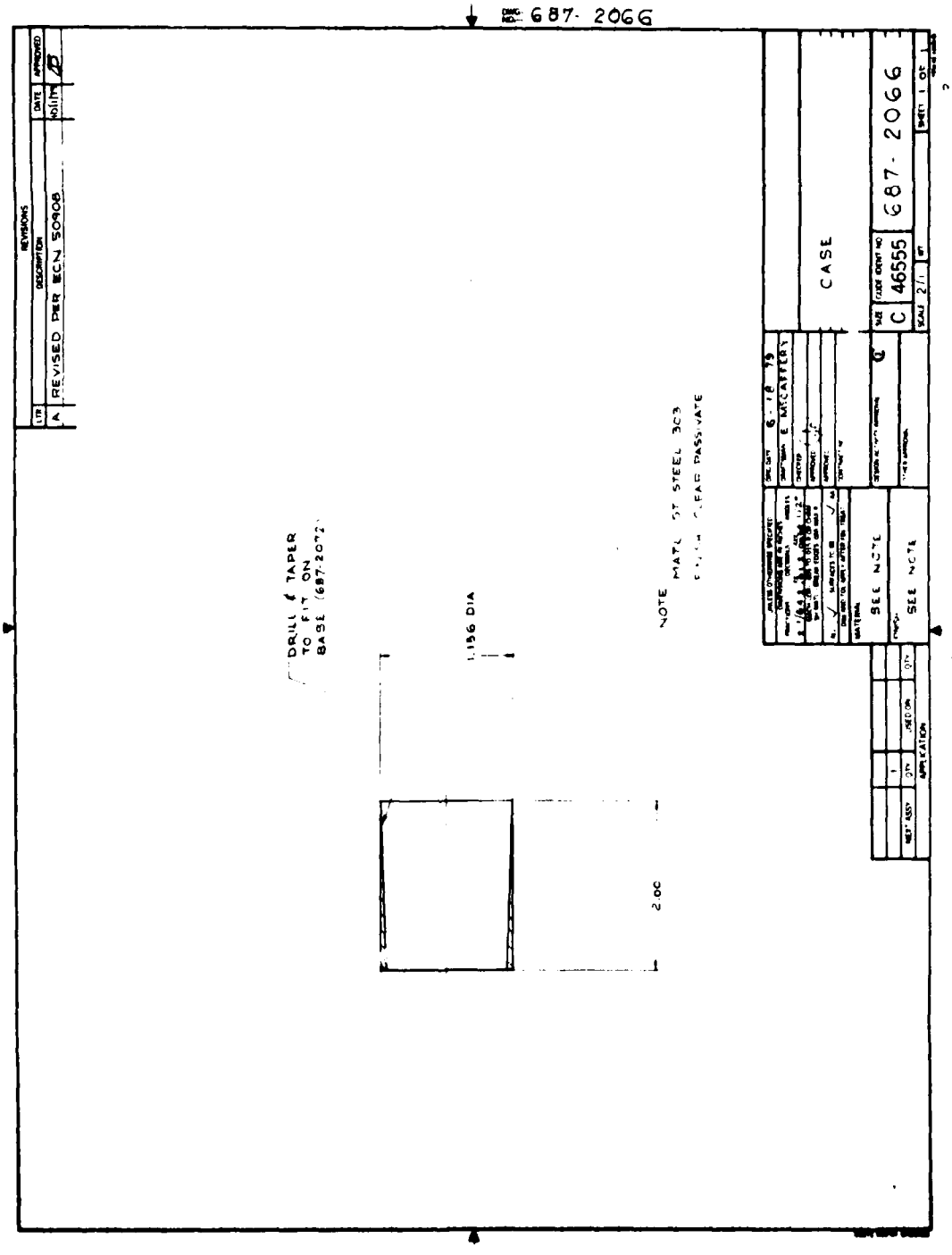

Figure A4. Case

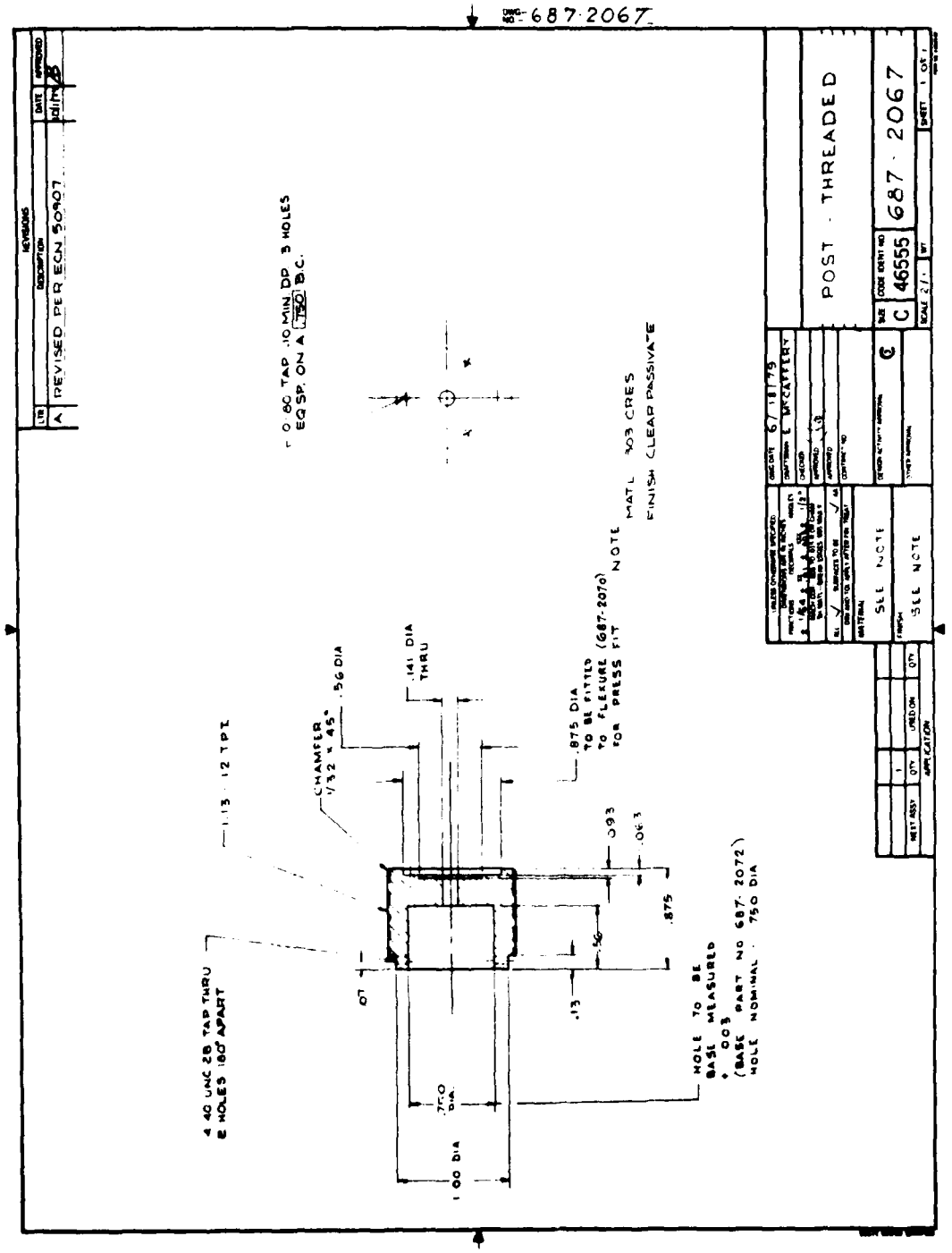

Figure A5. Post - Threaded

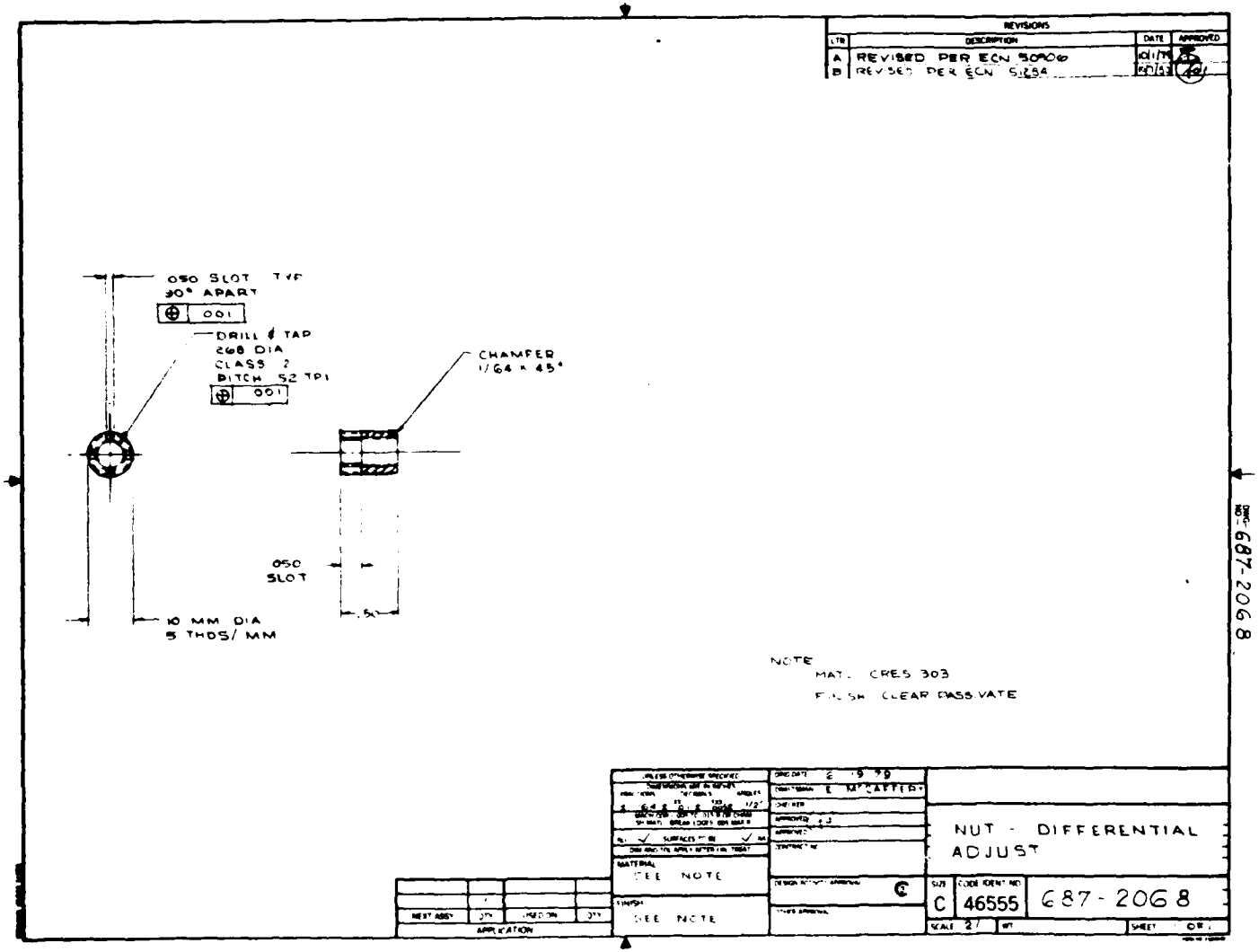

Figure A6. Nut - Differential Adjust

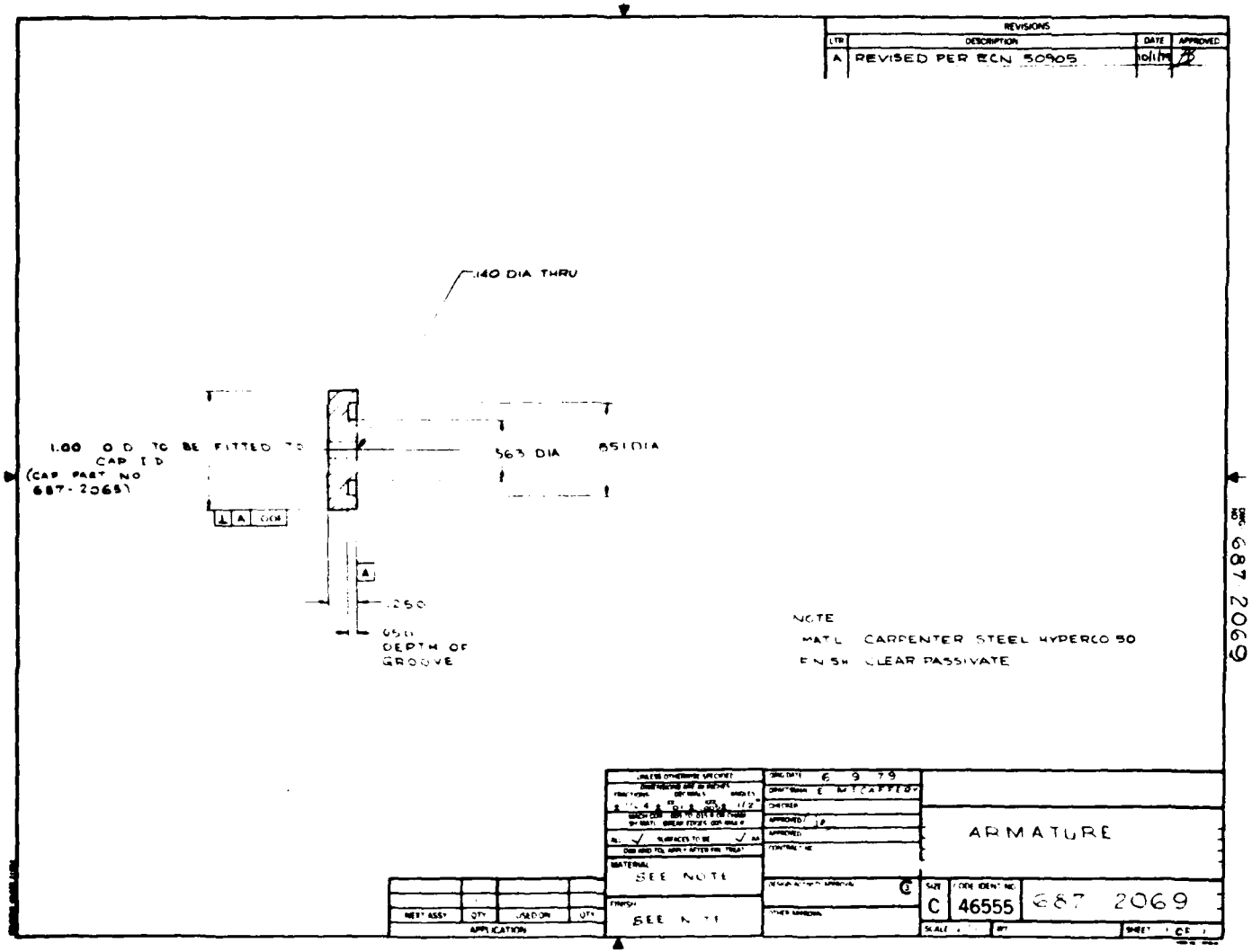

Figure A7. Armature

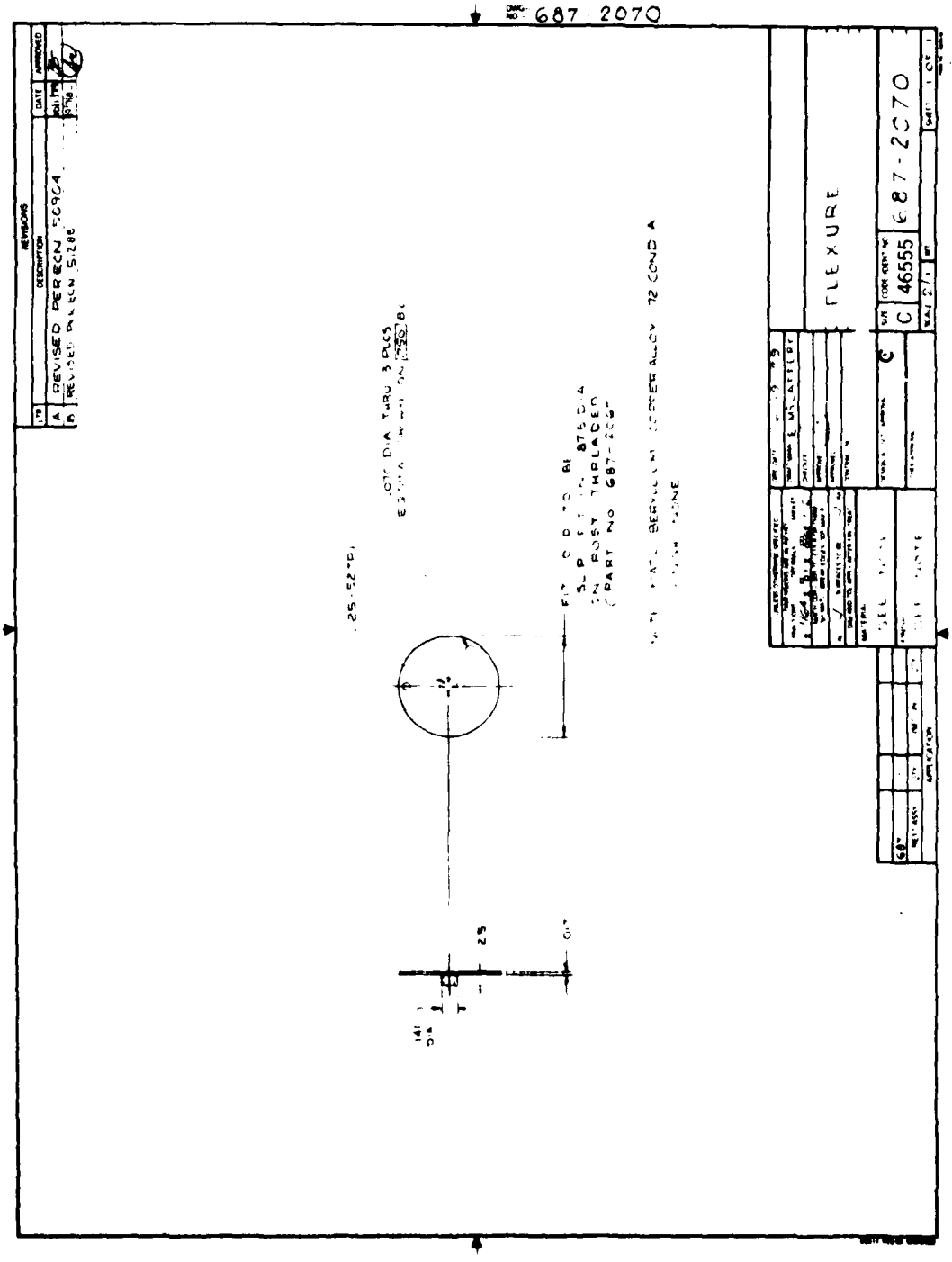

Figure A8. Flexure

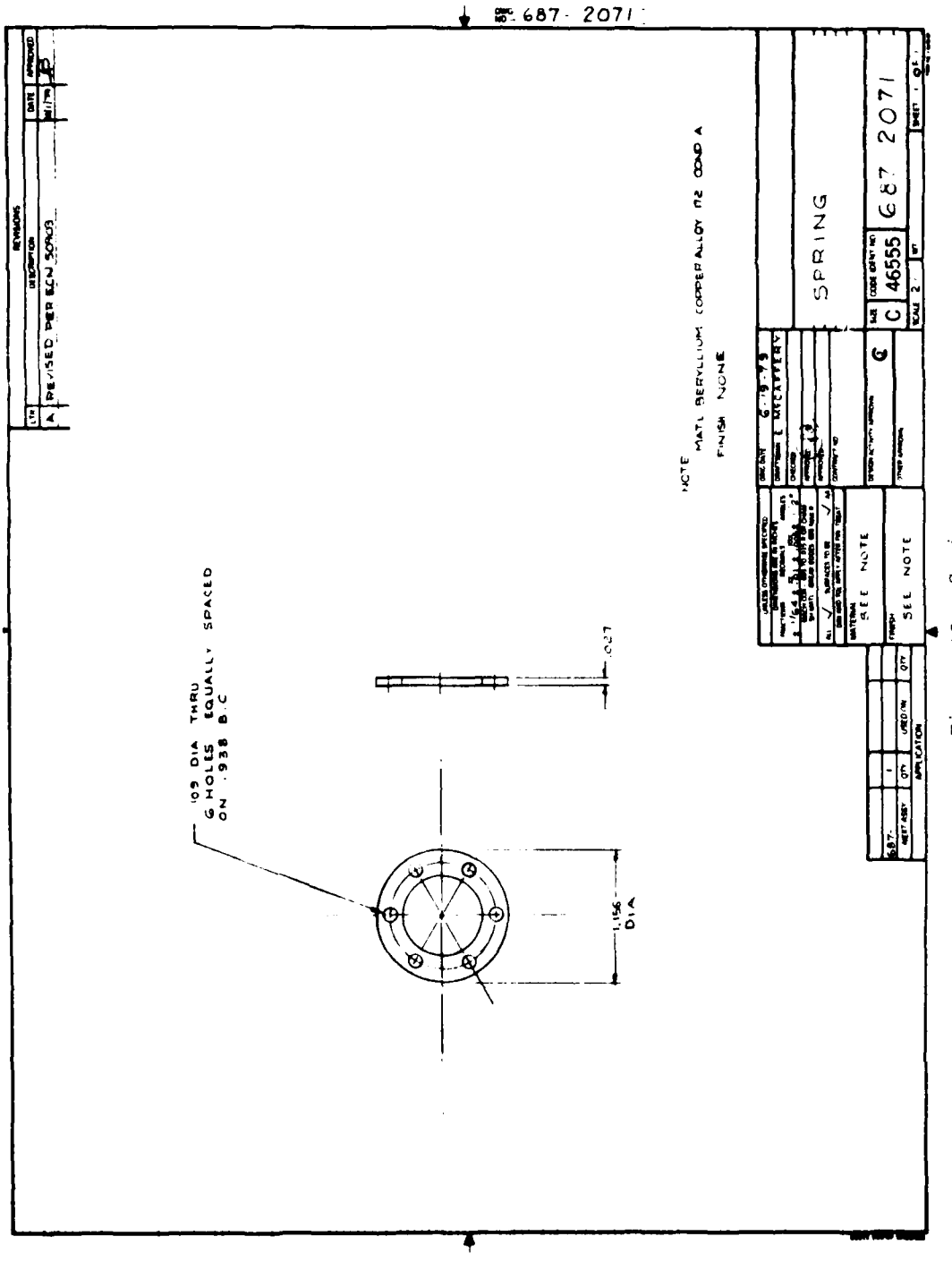

Figure A9. Spring

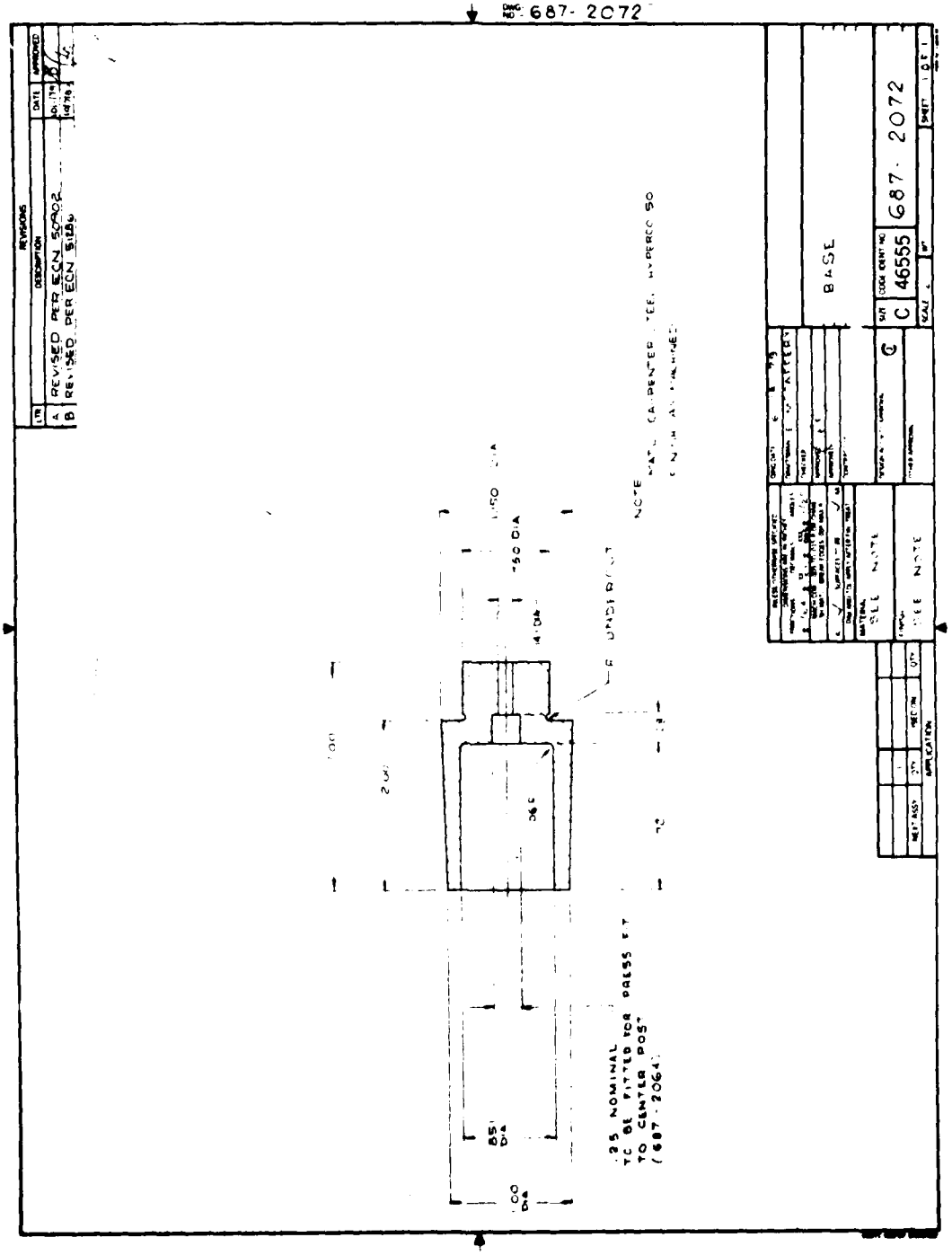

Figure A10. Base

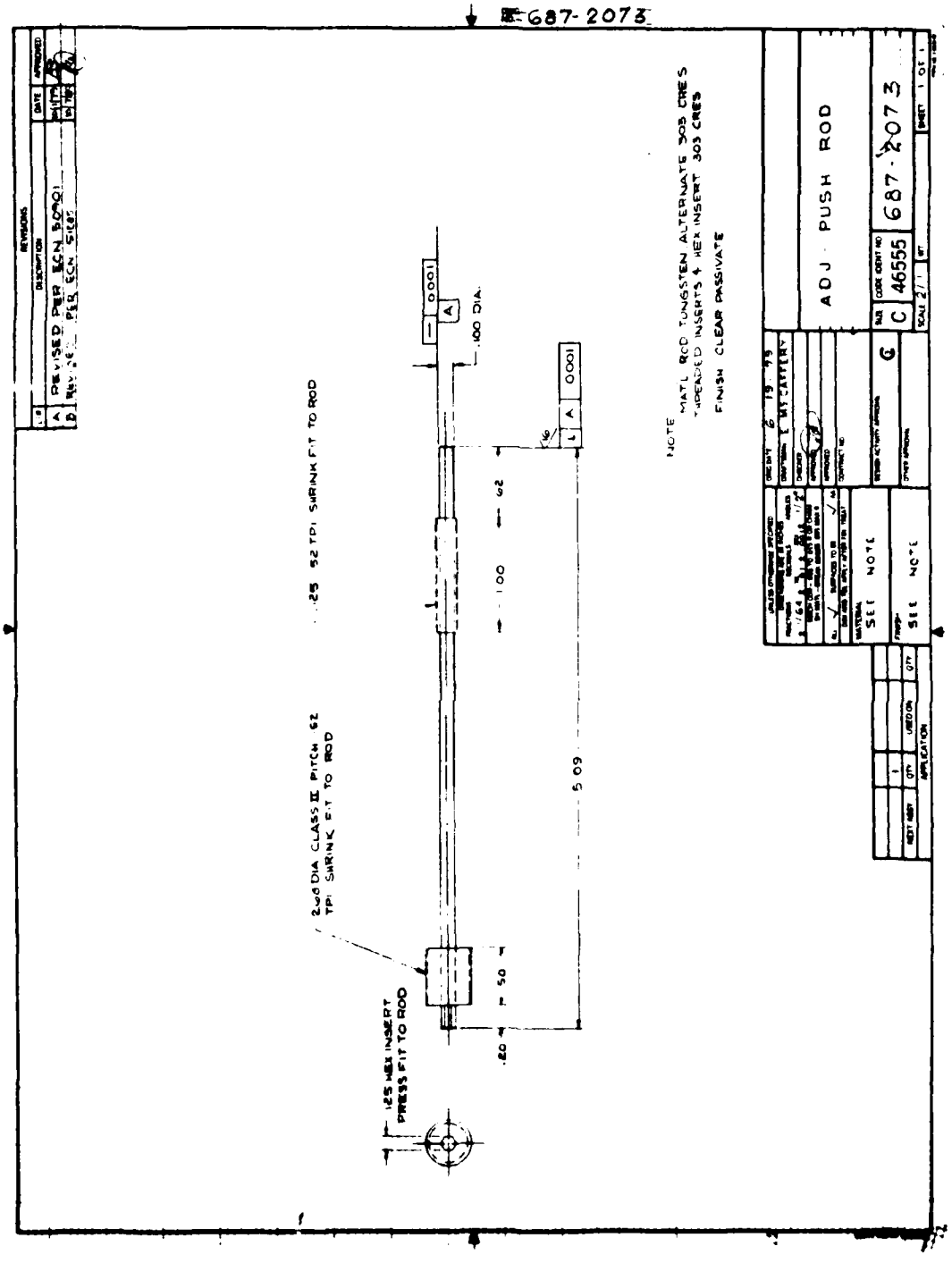

Figure All. Adj - Push Rod

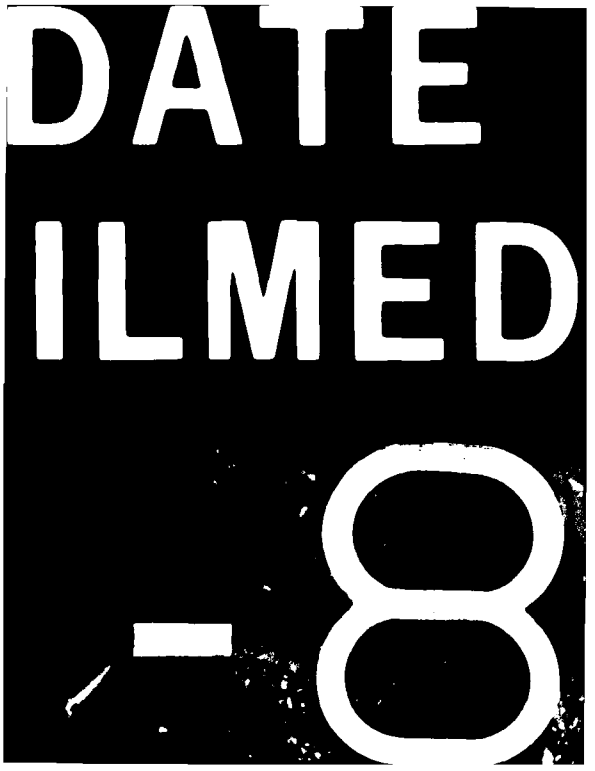
DATE
ILMED
-8